Study on aggregation mechanisms of a hydrogenotrophic methanogen, *Methanothermobacter* sp. CaT2, by characterization of aggregation mutants

KANA SUMIKAWA

Applied Molecular Bioscience

Graduate School of Medicine

Yamaguchi University

2020

CONTENTS

PAGE

LIST OF FIGURES i

LIST OF TABLES ii

ABBREVIATIONS iii

GENERAL INTRODUCTION 1

SUMMARY 4

CHAPTER 1

An Aggregation-defective Mutant of *Methanothermobacter* sp. CaT2 Reveals Unique Protein-dependent Aggregation

ABSTRACT 6

1.1 INTRODUCTION 7

1.2 MATERIALS AND METHODS 9

1.2.1 Strains and growth conditions 9

1.2.2 Phase-contrast, scanning electron microscope (SEM), and transmission electron microscope (TEM) images 9

1.2.3 Gas-phase analysis 10

1.2.4 Sedimentation index assay with various treatments 11

1.2.5 Extraction of genomic DNA 11

1.2.6 Genome sequencing and mapping analysis of CLA160 strains against CaT2 genome sequences 12

1.2.7 Sequence data deposition 13

1.2.8 Bioinformatics analyses 13

1.3 RESULTS 13

1.3.1 Characterization of the aggregating strain CaT2 and aggregation-defective mutant CLA160 13

1.3.2 Extracellular proteins related to CaT2 aggregation 19

1.3.3 Genomic analysis of the aggregation-defective mutant CLA160 21

1.3.4 Structure of the hypothetical protein encoded by MTCT_1020 21

1.3.5 Effects of DNase I and metal ions on the aggregation of CaT2 26

1.4 DISCUSSION 28

CHAPTER 2

Characteristics of physiology of and genomic mutations in aggregation-enhanced mutants of *Methanothermobacter* sp. CaT2

ABSTRACT 31

2.1 INTRODUCTION 32

2.2 MATERIALS AND METHODS 34

2.2.1 Strains and growth conditions 34

2.2.2 Observation under a phase-contrast, scanning electron microscope (SEM) and a transmission electron microscope (TEM) 34

2.2.3 Gas-phase analysis 35

2.2.4 Sedimentation index assay with various treatments 35

2.2.5 Extraction of genomic DNA 36

2.2.6 Genome sequencing and mapping analysis of CHA001 and CHA002 strains against CaT2 genome sequences 37

2.2.7 Sequence data deposition 38

2.3 RESULTS 38

2.3.1 Characterization of the aggregation-enhanced mutants CHA001 and CHA002 38

2.3.2 Aggregation of CHA001 and CHA002 mediated by extracellular proteins 44

2.3.3 Effects of DNase I and metal ions on aggregation of CHA001 and CHA002 44

2.3.4 Genomic analysis of mutations in CHA001 and CHA002 45

3.4 DISCUSSION 49

CONCLUSION 52

REFERENCES 53

LIST OF PUBLICATIONS 63

LIST OF FIGURES

CHAPTER 1

Fig. 1.1	Images of *Methanothermobacter* sp. CaT2 and aggregation-defective mutant CLA160	15
Fig. 1.2	Comparison of methane production between CaT2 and CLA160	16
Fig. 1.3	Sedimentation indexes of CaT2 and CLA160 and effect of proteinase K treatment	20
Fig. 1.4	Predicted domain architecture of *MTCT_1020* (T2GKU7, the mutated gene of CLA160), MTCT_0976 (T2GJL3), and MTCT_P1_0005 (T2GLL5) (CaT2), MTH_1074 (O27146) (ΔH), MTBMA_c14630 (D9PXU4) (*marburgensis*)	23
Fig. 1.5	Phylogeny of *MTCT_1020*-encoded protein and its homologues	24
Fig. 1.6	Effects of the DNase treatment or addition of metal ions on sedimentation indices of CaT2 and CLA160	27

CHAPTER 2

Fig. 2.1	Images of *Methanothermobacter* sp. CaT2 and the aggregation-enhanced mutants, CHA001 and CHA002	41
Fig. 2.2	Aggregation size of CaT2, CHA001, and CHA002	42
Fig. 2.3	Comparison of methane production by CaT2, CHA001, and CHA002	43
Fig. 2.4	Effects of proteinase K treatment, DNase treatment and addition of $CaCl_2$ on the sedimentation indices of CaT2 and CHA001	47
Fig. 2.5	Effects of proteinase K treatment, DNase treatment and addition of $CaCl_2$ on the sedimentation indices of CaT2 and CHA002	48

LIST OF TABLES

CHAPTER 1

Table 1.1	Summary of mutations in CLA160	17
Table 1.2	Thickness of cell wall (CW) and sugar layer (SL) in methanogen	18
Table 1.3	The hmmsearch using DUF17 model against *Methanothermobacter* protein sequences in Uniprot database	25

CHAPTER 2

Table 2.1	Thicknesses of the cell wall (CW) and sugar layer (SL) in aggregation-enhanced mutants CHA001 and CHA002	40
Table 2.2	Summary of mutations in CHA001 and CHA002	46

ABBREVIATIONS

dH_2O	Distilled water
ECPs	Extracellular polymers
eDNA	Extracellular DNA
EDTA	Ethylenediaminetetraacetic acid
EMS	Ethylmethane sulfonate
UASB	Upflow anaerobic sludge blanket

GENERAL INTRODUCTION

In everyday life, a tremendous amount of wastewater including organic materials is discharged after treatment by aerobic or anaerobic procedures for environmental protection. In the aerobic wastewater treatment, oxygen supply is essential but surplus sludge which causes industrial waste is generated, which means that a lot of carbon dioxide is emitted from fossil fuel (LaPara and Alleman, 1999), and the aerobic wastewater treatment is relatively expensive. On the other hand, the anaerobic wastewater treatment is methane fermentation, which needs no oxygen supply and thus generates less industrial waste (Seghezzo *et al*., 1998). As one of the wastewater treatments, an upflow anaerobic sludge blanket (UASB) reactor is utilized and the generated methane is used for energy in industry.

Methane fermentation by using the UASB reactor is performed by granules including fermenting bacteria, acetoclastic methanogens and hydrogenotrophic methanogens (Liu *et al*., 2002; Satoh *et al*., 2007; Schmidt *et al*., 1996; Sekiguchi *et al*., 1999). The methane fermentation process accumulates various intermediates, propionate, butyrate, succinate, and alcohol before producing acetate, hydrogen, carbon dioxide, and formate (Ahring, 1995; Schink, 1997). Propionate is known as an organic substance that is difficult to decompose in the methane fermentation. It is also known that the accumulation of propionate, acetate, and butyrate, called as volatile fatty acids (VFAs), in reactors causes a decrease of methane production (Kaspar and Wuhrmann, 1978a; Kaspar and Wuhrmann, 1978b; Ueno *et al*., 2001). The efficient degradation of VFAs is related to the activity of granules and also to the efficiency of fermentation on a UASB reactor and the shorter lag time on reactor start-up (Hulshoff Pol *et al*., 2004; Liu *et al*., 2003; Schmidt *et al*., 1996). Fermentation in the UASB reactor is carried out under mesophilic (approximately 37°C) or thermophilic (approximately 55°C) conditions. The granule formation in mesophilic reactors is stable than that in thermophilic reactors. However, methane production

in thermophilic reactors is 2- to 3-times higher than that in mesophilic reactors (Orell *et al*., 2013; Harada *et al*., 2014; Van Lier *et al*., 1996).

Methane productivity depends on granules formation. A core of granule consists of methanogens and fermentative microorganisms coated around the methanogens (Sekiguchi *et al*., 1999). The aggregation of thermophilic methanogens is thus important for the stabilization of granules and for the stable thermophilic methane fermentation. Among microorganisms, various substances such as extracellular DNA (eDNA), proteins, lipids, and polysaccharides are known to be involved in aggregation (Flemming *et al*., 2010; Liu *et al*., 2003; Liu *et al*., 2004; Okshevsky *et al*., 2015; Orell *et al*., 2013; Veiga *et al*., 1997). In the environment, biofilm is known as one of aggregation styles of microorganisms (Claessen *et al*., 2014; Flemming *et al*., 2010), and the cell-to-cell communication called quorum sensing (QS) that recognizes the population density coordinates the switch to a biofilm lifestyle (Solano *et al*., 2014). Biofilm seems to protect cells from environmental stresses and to reserve nutrients (LaPaglia and Hartzell, 1997). The biofilm of *Archaeoglobus fulgidus*, an anaerobic marine hyperthermophile, is composed of polysaccharides, proteins, and metals (LaPaglia and Hartzell, 1997). In the presence of Cu^{2+} and Zn^{2+}, *A. fulgidus* induces biofilm formation (LaPaglia and Hartzell, 1997).

Aggregation substances and mechanisms have been reported in several mesophilic methanogens. *Methanobacterium formicicum* and *Methanotbrevivacter* sp. produce extracellular polymers (ECPs) to connect with other aggregated species (Schmidt *et al*., 1996; Veiga *et al*., 1997). *Methanosarcina mazei* produces polysaccharide-based extracellular polymers to attach to the cells (Robinson *et al*., 1985). *Methanococcus maripaludis* produces flagella and pili to adhere to other microbes (Jarrell *et al*., 2011). However, little is known about the aggregation of thermophilic methanogens.

One of thermophilic hydrogenotrophic methanogen, *Methanothermobacter* sp. CaT2 is aggregated itself and with other microorganisms (Kosaka *et al*., 2014). Physiological analysis on

CaT2 has suggested that the cell-surface sugar layer, which is assembled by glycosyltransferases, is related to the aggregation (Kosaka *et al*., 2014). CaT2 exhibits a syntrophic association with a syntrophic propionate-oxidizing bacterium, *Pelotomaculum thermopropionicum* SI (Kosaka *et al*., 2014) that has flagellum-like filaments (Ishii *et al*., 2005). The co-culture of CaT2 and SI shows efficient propionate degradation to methane compared with that of non-aggregated methanogen and SI (Kosaka *et al*., 2014), suggesting that the aggregation of methanogen plays an important role in efficient propionate degradation by the association with SI.

In this study, an aggregation-defective mutant, CLA160 and aggregation-enhanced mutants, CHA001 and CHA002, as shown in chapters 1 and 2, respectively, were isolated to clarify the aggregation mechanisms of CaT2 (Sumikawa *et al*., 2019; Sumikawa *et al*., 2020). The sugar layer of CLA160 and CHA002, and the cell wall of CHA001 and CHA002 were thinner than that of CaT2. The genomic sequence analysis of CLA160 revealed that MTCT_1020 coding a hypothetical protein has a non-sense mutation to cause large deletion of the protein. The mutation seems to be responsible for the aggregation-defective phenotype because proteinase K treatment showed no effect on the sedimentation index of CLA160 (see chapter 1). On the other hand, proteinase K treatment almost completely reduced the sedimentation index of CHA001 as in the case of CaT2 but reduced the sedimentation index of CHA002 to some extent but not completely (see chapter 2). Mutation(s) in CHA002 may thus lead to exhibit non-proteinous aggregation. The addition of Ca^{2+} enhanced the aggregation of CaT2, CHA001, and CHA002 but not of CLA160. Therefore, it is likely that main factor(s) responsible for the CaT2 aggregation is extracellular protein(s), whose function(s) is enhanced by Ca^{2+}, and ancillary factor(s) is non-proteinous material(s) such as the surface sugar layer. These findings may provide new insights into the aggregation of not only *Methanothermobacter* sp. but also other methanogens or bacteria.

SUMMARY

Study on aggregation mechanisms of a hydrogenotrophic methanogen, *Methanothermobacter* sp. CaT2, by characterization of aggregation mutants

A formation of granules plays an important role for the stable operation of an upflow anaerobic sludge blanket (UASB) type methane fermentation reactor. Granule formation involves many kinds of microorganisms that perform methane fermentation, and aggregating methanogens are also thought to play an important role. Especially, it has been reported that hydrogenotrophic methanogens enhance the substrate oxidation by syntrophic association with fermenting bacteria, and the aggregation is considered to be involved in the symbiotic relationships. Since the genetic engineering method for hydrogenotrophic methanogens has not been established yet, surface sugar layer relationship to the aggregation was already reported. Furthermore, eDNA and protein were reported in other methanogens aggregations. In this study, aggregation mutants are obtained from the aggregating hydrogenotrophic methanogen, *Methanothermobacter* sp. CaT2, which are CLA160 with reduced aggregation and CHA001 and CHA002 with increased aggregation. In addition, the results of physiological analyses and genomic sequencing of these mutants give us information on the aggregation mechanisms of CaT2.

When the cultured cells were treated with protease, CaT2, CLA001, and CHA002 showed decreased aggregation, but CLA160 had almost no effect. In addition, CHA002 did not completely reduce the aggregation by the protease treatment. These results suggest that the aggregation of CaT2 involved of non-proteinous materials. The genomic sequence analysis of CLA160 revealed that *MTCT_1020*, coding hypothetical protein, contained a non-sense mutation causing largely deletion. The structural analysis predicted that MTCT_1020 displayed on the cell

surface, suggesting that CaT2 forms aggregation by this protein. On the other hand, the genomic sequence analysis of CHA001 and CHA002 confirmed mutations to several genes in both strains, indicating that the mutations in the genome enhanced its aggregation. These results suggest that extracellular protein, MTCT_1020, is mainly involved in the aggregation of CaT2, but non-proteinous materials are also involved in the aggregation.

CHAPTER 1

An Aggregation-defective Mutant of *Methanothermobacter* sp. CaT2 Reveals Unique Protein-dependent Aggregation

ABSTRACT

The thermophilic hydrogenotrophic methanogen, *Methanothermobacter* sp. CaT2, which possesses an extracellular sugar layer, commonly aggregates by itself or with other microorganisms. To elucidate the molecular mechanisms responsible for this aggregation, the aggregation-defective mutant, CLA160, was isolated. Optical and electron microscopy observations revealed that the mutant exhibited a significant reduction in aggregation. Genomic sequencing showed that CLA160 has a single point mutation, causing a nonsense mutation in MTCT_1020, which encodes a hypothetical protein. Motif and domain analyses indicated that the hypothetical protein bears two membrane-spanning segments at the N- and C-terminal regions and a large middle repeat-containing region. The results of a bioinformatic analysis suggested that the first middle region (RII) of the protein or the whole structure is responsible for the function of the product of MTCT_1020 in the aggregation of CaT2. A treatment with proteinase K suppressed sedimentation in CaT2, indicating a reduction in aggregation, with almost no effect on sedimentation in CLA160. The addition of Ca^{2+} or Mg^{2+} ions enhanced sedimentation in CaT2, whereas a DNase treatment had no effect on sedimentation in either strain. These results suggest that the hypothetical protein encoded by MTCT_1020 plays a key role as a membrane-bound adhesion protein in the aggregation of CaT2, which is enhanced by the addition of Ca^{2+} or Mg^{2+} ions.

1.1 INTRODUCTION

Methane fermentation is performed under mesophilic (approximately 37°C) or thermophilic (approximately 55°C) conditions in bioreactors, among which the upflow anaerobic sludge blanket (UASB) reactor is the most widely and effectively used (Schmidt *et al*., 1995; Uemura S. and H. Hrada, 1993). Efficient fermentation in UASB-type reactors depends on the formation and activity of granules (Liu *et al*., 2003; Schmidt *et al*., 1996). Granules are composed of many types of microorganisms, including primary fermenting bacteria, secondary fermenting bacteria, acetoclastic methanogens, and hydrogenotrophic methanogens (Liu *et al*., 2003; Satoh *et al*., 2007; Schmidt *et al*., 1996; Sekiguchi *et al*., 1994). Methanogens are considered to be key species in granule formation (Fernández *et al*., 2008; Uemura S. and H. Hrada, 1993; Zinder *et al*., 1984). Methanogens in the granules that form in thermophilic reactors produce two- to three-fold more methane than methanogens in granules in mesophilic reactors (Harada *et al*., 2004; Orell *et al*., 2013). However, granule formation is generally more difficult in thermophilic reactors than in mesophilic reactors (Harada *et al*., 2004). This phenomenon may be attributed to stability differences in aggregation mechanisms or responsible molecules under mesophilic and thermophilic conditions. Therefore, a clearer understanding of the aggregation mechanisms of thermophilic methanogens is important when considering the stabilization of UASB reactors. Cellular aggregation has been reported in many microorganisms; it is accomplished via aggregating substances, such as filaments, extracellular DNA (eDNA), proteins, lipids, and polysaccharides (Flemming *et al*., 2010; Liu *et al*., 2003; Liu *et al*., 2004; Orell *et al*., 2013; Veiga *et al*., 1997). Several aggregating methanogens, particularly mesophilic methanogens, have been reported to date, and their aggregation substances and mechanisms have been investigated. *Methanosarcina mazei* produces polysaccharide aggregates and forms extracellular polymers (ECPs) that attach to the outer surfaces of cells (Robinson *et al*., 1985).

Methanobacterium formicicum and *Methanobrevibacter* sp. produce ECPs to bridge the gap between aggregates formed by other species (Schmidt *et al*., 1996; Veiga *et al*., 1997). *Methanococcus maripaludis* uses flagella and pili to adhere to the surfaces of other microbes (Jarrell *et al*., 2011). Therefore, mesophilic methanogen aggregation mechanisms using polysaccharides, ECPs, and proteins have been proposed. However, research on aggregating thermophilic methanogens is limited. The thermophilic aggregating hydrogenotrophic methanogen, *Methanothermobacter* sp. CaT2, was recently reported (Kosaka *et al*., 2014). A physiological analysis of CaT2 suggested that its cell-surface sugar layer is responsible for its aggregation properties (Kosaka *et al*., 2014). The genome of this self-aggregating thermophilic methanogen has been sequenced and its genetic background revealed (Kosaka *et al*., 2013). A comparative genomic analysis with other thermophilic hydrogenotrophic methanogens indicated that CaT2 contains specific aggregation related adhesion genes and suggested that pili (fimbriae) do not affect strong cell-to-cell aggregation of CaT2 (Kosaka *et al*., 2014). However, no clear relationship between the physiology and genetics of CaT2 has been identified, and its aggregation mechanisms currently remain unclear. In order to elucidate the molecular mechanisms underlying the cell-to-cell aggregation of CaT2 in more detail, we isolated the mutant, CLA160, which displayed significantly decreased aggregation. A mutation analysis revealed that CLA160 has a nonsense mutation in a gene for a hypothetical membrane protein with a large extracellular domain. In addition, a proteinase K treatment suggested that proteins on the membrane or cell wall are responsible for aggregation in CaT2.

1.2 MATERIAL AND METHODS

1.2.1 Strains and growth conditions

Methanothermobacter sp. CaT2 (DSM 24414 and NBRC 107770) and its mutant derivatives were used in the present study. Strains were grown in W medium at 55°C as previously described (Kosaka *et al*., 2014), or W-R medium (W medium without resazurin solution) under a controlled atmosphere: 160 kPa H_2/CO_2 (80/20 [v/v]) (Sumitomoseiki, Osaka, Japan). The aggregation-defective mutant CLA160 was isolated as follows. To increase mutation frequency, ethyl methanesulfonate (EMS) was used as a mutagen. The EMS treatment was performed according to a previously reported method (Watrin *et al*., 1996). EMS was added to a culture of CaT2 at a final concentration of 0.5 M and cells were incubated at 37°C. Cells in the culture were collected by centrifugation and washed once with a 6% w/v sodium thiosulfate solution, washed twice with dH_2O, and inoculated into fresh W-R medium under H_2/CO_2 (80/20 [v/v]). Mutagen-treated cells were passed through a 5-μm filter to remove aggregated cells and the cell suspension was then centrifuged. The pellet was suspended in 1 mL of dH_2O and 100 μL of the suspension was mixed in W medium gellan gum plates for colonies to grow following a previously described method (Nakamura *et al*., 2011). Each colony was then grown in W medium under H_2/CO_2 (80/20 [v/v]) and aggregation was examined several times using a phase-contrast microscope (Eclipse E600; Nikon, Tokyo, Japan) to check the characteristics of the mutants.

1.2.2 Phase-contrast, scanning electron microscope (SEM), and transmission electron microscope (TEM) images

A fluorescence microscope (Eclipse E600; Nikon) was used to take phase-contrast images. SEM images were taken using the following procedure: Cell pellets were fixed for 3 h with 1.25% glutaraldehyde in 0.1 M cacodylate buffer (pH 6.5) at 4°C, washed with 0.1 M

cacodylate buffer, and then suspended with a small amount of the same buffer. The suspension was dropped on a 0.2-μm cellulose membrane filter and dehydrated with a graded ethanol series and t-butyl alcohol. The dehydrated filter was dried using vacuum freeze-drying equipment (VFD-21S; Vacuum Device, Ibaraki, Japan). The dried membrane filter was then coated with platinum (Auto Fine Coater, JFC-1600; JEOL, Tokyo, Japan). Images of sections were obtained by observations using SEM (10 kV, 30 μs; JSM-6360LA; JEOL). TEM with ruthenium red was performed as previously described (16), with slight modifications. Cell pellets were fixed for 5 h with 1.25% glutaraldehyde and 0.5 mg mL−1 ruthenium red in 0.1 M cacodylate buffer (pH 6.5) at 4°C, washed in 0.1 M cacodylate buffer, and post-fixed for 2 h in 1% osmium tetroxide containing 0.5 mg mL−1 ruthenium red in 0.1 M cacodylate buffer at 4°C. After being rinsed with 0.1 M cacodylate buffer, the pellets were embedded in a 3% agarose gel and dehydrated with a graded ethanol and acetone series. The dehydrated blocks were embedded in Epok 812 (Kohken, Tokyo, Japan). Ultra-thin sections were cut using a diamond knife mounted in an ultramicrotome (EM-UC6; Leica, Wetzlar, Germany), then placed on copper grids and stained with uranyl acetate and lead citrate. TEM examinations were performed using a Tecnai G2 Spirit electron microscope (Thermo Fisher Scientific, Massachusetts, USA) at an acceleration voltage of 80 kV.

1.2.3 Gas-phase analysis

Methane and hydrogen were analyzed using a gas chromatography system (GC-8A and C-R6A; Shimadzu, Kyoto, Japan) with a thermal conductivity detector and column (2 m×3 mm stainless steel) packed with Unibeads C 60–80 (GL Science, Tokyo, Japan). Analysis conditions were as follows: injection at 150°C, column at 145°C, detector at 150°C, current for the detector at 50 mA, and flow rate of carrier Ar gas at 30 mL min^{-1}.

1.2.4 Sedimentation index assay with various treatments

Cells strains were grown in W-R medium at 55°C for 4 d under H_2/CO_2 (80/20 [v/v]), recovered by centrifugation, washed twice, and suspended in 10 mM Tris-HCl buffer (pH 7). Suspensions (OD600 ca. 0.7–1.5) were subjected to optical density measurements or to the following treatments. In the proteinase K treatment, proteinase K (Wako Pure Chemical Industries, Osaka, Japan) was added to the cell suspension at a final concentration of 10 μg mL^{-1} and the solution was incubated at 37°C for 1 h. The control examination was performed by the addition of 10 mM Tris-HCl buffer instead of proteinase K. After the incubation, cells were washed once with 1 mL of 10 mM Tris-HCl buffer and subjected to a sedimentation index assay. Regarding the DNase I, $CaCl_2$, and $MgCl_2$ treatments, DNase I, $CaCl_2$, $MgCl_2$, or Tris-HCl buffer was added to the cell suspension at a final concentration of 5 μg mL^{-1}, 10 mM, 10 mM, and 10 mM, respectively, and solutions were incubated at 37°C for 1 h. The control examination was performed by adding 10 mM Tris-HCl buffer instead of DNase I, $CaCl_2$, or $MgCl_2$. After the incubation, cells were washed once and suspended in 10 mM Tris-HCl buffer. To compare the speed of the sedimentation of cells, these cell suspensions were mixed briefly and their turbidity was measured at OD600 every 10 mins for 50 min using a photometer (Libra S12; Berthold Technologies, Bad Wildbad, Germany). The sedimentation index was calculated using the following equation: Sedimentation index = (the value of turbidity at each measured time) / (the value of turbidity at 0 min) × 100.

1.2.5 Extraction of genomic DNA

Cells were grown in 500 mL of W medium at 55°C for 4 d under H_2/CO_2 (80/20 [v/v]), recovered by centrifugation (12,000 rpm) at 4°C for 15 min, and washed twice with dH_2O. Cell pellets were suspended in TE buffer. The suspension was then subjected 5 times to a freeze-thaw treatment of freezing at –80°C for 30 min and thawing at 55°C for 10 min. The treated solution

was incubated overnight at 55°C following the addition of SDS, proteinase K, NaCl, and RNase A, at final concentrations of 0.5% (w/v), 100 μg mL^{-1}, 10 mM, and 10 μg mL^{-1}, respectively. After the incubation, the solution was gently mixed by inversion with double the volume of TE-saturated phenol. A half-volume of chloroform was added, and the solution was kept on ice for 5 min before being centrifuged at 14,000 rpm for 15 min at 4°C. Sodium acetate (pH 8) was then added to the transferred upper aqueous layer to a final concentration of 0.3 M. The solution was gently mixed with an equal volume of isopropanol and centrifuged at 14,000 rpm for 15 min at 4°C. The precipitate was washed with an equal volume of 70% (v/v) ethanol and centrifuged at 14,000 rpm for 15 min at 4°C. The resultant precipitate was dried and resuspended in 100 μL of TE buffer. The sample of genomic DNA was further purified using a Genomic-tip 20 kit (Qiagen, Hilden, Germany), according to the manufacturer's instructions.

1.2.6 Genome sequencing and mapping analysis of CLA160 strains against CaT2 genome sequences

We previously reported the complete genome sequence for the *Methanothermobacter* sp. CaT2, which is available at DDBJ/EMBL/ GenBank, accession numbers AP011952.1 and AP011953.1 (Kosaka *et al*., 2013). To identify the mutation sites of CLA160, we performed genome sequencing of CLA160 using the Illumina Hiseq 2000 platform and mapped this against the complete genome sequence of CaT2. The genome sequencing of CLA160 was performed as previously reported (Matsutani *et al*., 2014). A total of 6,207,761 sequence pairs of 100 bp paired-end nucleotide reads from CLA160 were obtained, which yielded approximately 717-fold sequence coverage. The Illumina sequencing reads of CLA160 were aligned with the CaT2 genome sequence using BWA (Li *et al*., 2009). Mutation sites were searched for using the Genome Analysis Toolkit (GATK) v 2.1.8 (McKenna *et al*., 2010). Predicted mutation sites were analyzed by direct sequencing using appropriate primers: for 1022836, CLAm02_F: GAATATGGGTCTCGCCGTTA, CLAm02_R: AGG TAATGGCACCATTTCAGG; for 1180340,

CLAm13_F: CCGA TACAGAGAAGACCCTCC, CLAm13_R: CAGCATATTACTTG AGGCGACAG; and for 1614615, CLAm14_F: CACAAGTGCC TTCATGGTTAC, CLAm14_R: TGTCTCATGCACACATCACC. Direct sequencing was performed using an ABI 3130XL sequencer (Applied Biosystems, California, USA) with a Big Dye Terminator v3.1 Cycle Sequencing Kit (Applied Biosystems), according to the manufacturer's instructions.

1.2.7 Sequence data deposition

Illumina sequence reads of the CLA160 strain have been deposited in the DDBJ Sequence Read Archive under the accession number DRA006429. The BioProject ID of the CAL160 strain is PRJDB6667.

1.2.8 Bioinformatics analyses

An HMM model search was performed by hmmsearch using the HMMER web server (https://www.ebi.ac.uk/Tools/hmmer/search/ hmmsearch) (Finn R.D. *et al*., 2011, Finn R.D. *et al*., 2015). DELTA-BLAST was performed using the NCBI web server (https://blast.ncbi.nlm.nih.gov/Blast.cgi). The selection of similar proteins from the DELTA-BLAST result was performed using a ruby script under the condition: E-value<1.0e−10, sequence coverage >85%, identity >20%.

1.3 RESULTS

1.3.1 Characterization of the aggregating strain CaT2 and aggregation-defective mutant CLA160

Methanothermobacter sp. CaT2 cells exhibited strong aggregation in W medium. The sugar layer on the cell surface of CaT2, which was stained by ruthenium red, was assumed to

contribute to the aggregation of CaT2 (Kosaka *et al*., 2014). To elucidate the mechanisms underlying CaT2 aggregation, the aggregation-defective mutant, CLA160, was obtained. Since there are no methods for gene engineering, including gene disruption, in *Methanothermobacter* sp., an EMS treatment was applied for the acquisition of aggregation-defective mutants. Following cultivation, one of these mutants, CLA160, was compared with the parental strain, CaT2, using microscopy. Phase-contrast images indicated that CaT2 and CLA160 showed significant aggregation and almost no aggregation, respectively (Fig. 1.1 A and B). SEM observations revealed that individual cells of CaT2 bound with other cells via interactions at their long axes, whereas CLA160 cells showed no such interactions (Fig. 1.1 C and D). TEM revealed that CaT2 and CLA160 both exhibited similar smooth cell-surface structures (Fig. 1.1E and F). Moreover, sugar staining observations indicated that the sugar layer was slightly thinner, but still present, on CLA160 (Fig. 1.1 G and H, Table 1.2). However, no significant difference in the thickness of the cell wall including the surface layer (S-layer) was found between CaT2 and CLA160 (Table 1.2). The colony morphology of CLA160 was similar to that of CaT2, in which the cell was surrounded by a mycelium-like structure. However, the colony size of CLA160 was slightly smaller than that of CaT2 (data not shown). These results indicated that CLA160 is clearly aggregation-defective and that CaT2 has an unidentified mechanism for cell-to-cell aggregation. Notably, methane production by CLA160 was found to be of the same level and pattern as that by CaT2 under agitation (Fig. 1.2), suggesting that the mutation does not affect the central metabolism of CLA160.

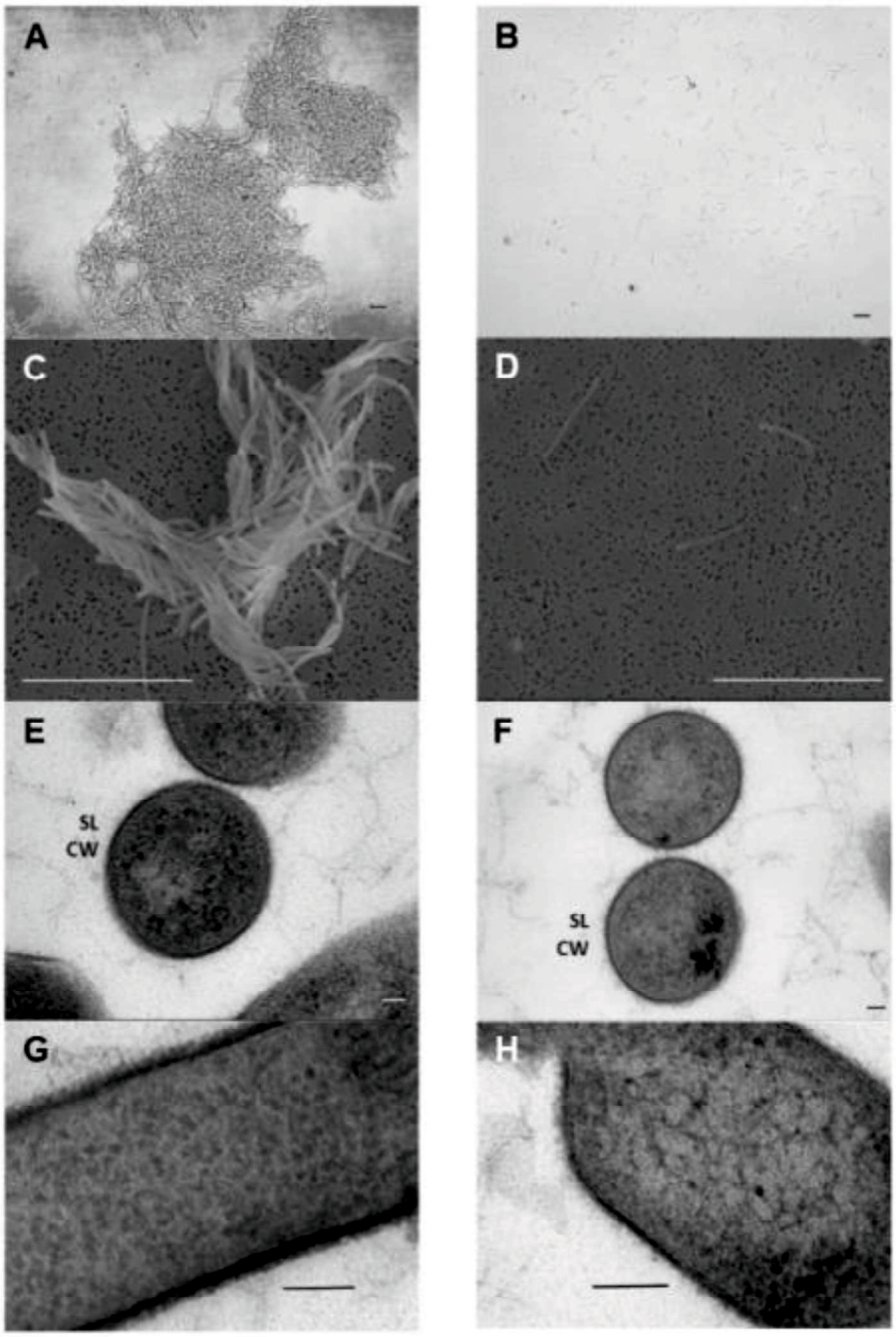

Fig. 1.1 Images of *Methanothermobacter* sp. CaT2 and aggregation-defective mutant CLA160 Phase-contrast images of CaT2 (A) and CLA160 (B) were taken at a 400× magnification. SEM images of CaT2 (C) and CLA160 (D) were taken at a 12,000× magnification. TEM images of CaT2 (E, G) and CLA160 (F, H). SL, surface layer; CW, cell wall. Bars represent 10 μm in A, B, C, and D; 50 nm in E and F and 100 nm in G and H.

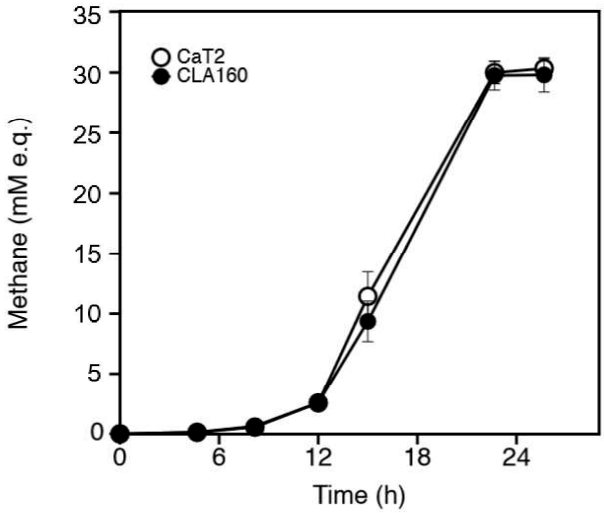

Fig. 1.2 Comparison of methane production between CaT2 and CLA160

CaT2 (open circle) and aggregation-defective mutant CLA160 (closed circle) were grown in W medium under H_2–CO_2 (80:20, v/v) and the methane production was measured. Error bars represent standard deviations of the means of two independent experiments.

Table 1.1 Summary of mutations in CLA160

Position	Gene	Product	Mutation	Amino acid substitution	Amino acid number
1022836	*MTCT_1020*	Hypothetical protein	Nonsense mutation C→A	Gly166Stop	144
1180340	non-coding	—	Deletion T	—	—
1614615	non-coding	—	Nucleotide substitution G→T	—	—

Table 1.2 Thickness of cell wall (CW) and sugar layer (SL) in methanogen

Strain	CW*	SL*
CLA160	15.6 ± 1.3	8.8 ± 0.63
CaT2	15.2 ± 1.3	12.7 ± 0.8

*Thickness of the layer structure was measured from each TEM image. Standard deviations are indicated after. n = 20.

1.3.2 Extracellular proteins related to CaT2 aggregation

Previous studies indicated that biofilm-forming archaea, such as *Methanobrevibacter smithii* and *Sulfolobus solfataricus*, produce an abundant extracellular matrix, mainly composed of polysaccharides and proteins, surrounding their cells (Orell *et al*., 2013). To examine whether extracellular proteins are involved in the aggregation of CaT2, a proteinase K treatment experiment was performed, and its effects were evaluated by sedimentation experiments. CaT2 showed a large reduction in the sedimentation index, whereas CLA160 showed almost no difference (Fig. 1.3), which is consistent with previous findings showing that aggregated cells sediment markedly faster than nonaggregated cells (Kosaka *et al*., 2013). Phase-contrast observations confirmed that the proteinase K treatment caused the dispersion of CaT2 aggregated cells (data not shown). These results suggest that CaT2 has extracellular proteins that are responsible for aggregation, and also that the genes coding for these proteins are defective in CLA160.

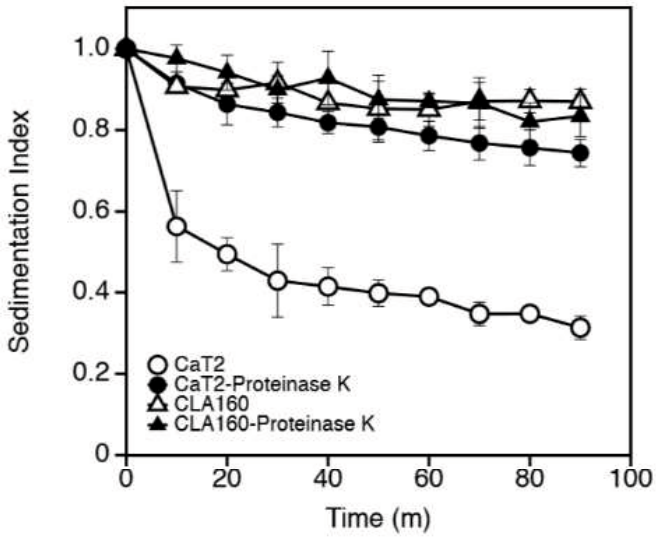

Fig. 1.3 Sedimentation indexes of CaT2 and CLA160 and effect of proteinase K treatment

CaT2 (circle) and aggregation-defective mutant CLA160 (triangle) were treated with proteinase K (closed) or left untreated (open) and then subjected to sedimentation analysis. Error bars represent standard deviations of the means of three independent experiments.

1.3.3 Genomic analysis of the aggregation-defective mutant CLA160

To identify genes encoding for extracellular proteins related to the aggregation of CaT2, CLA160 was subjected to draft genome sequencing followed by direct sequencing. Three single-nucleotide mutations were found in CLA160 (Table 1.1). Two of them occurred in a non-coding region and the remaining one in the gene MTCT_1020, which encodes a hypothetical protein with 3,162 amino acid residues. The mutation in MTCT_1020 was a single nucleotide substitution that caused a nonsense mutation, resulting in a reduction in the size of the product to 144 amino acid residues. Taken together with the results from the experiments with proteinase K, the product of MTCT_1020 appears to have lost its function in CLA160 and is responsible for aggregation in CaT2.

1.3.4 Structure of the hypothetical protein encoded by MTCT_1020

To understand the function of the hypothetical protein encoded by MTCT_1020, the protein sequence structure, particularly at the motif and domain levels, was analyzed. Information in the database showed a signal sequence at its N terminus, a carboxypeptidase-like domain (IPR008969) (RI), a large middle region containing repeated domains separated into two portions (RII: FunFam 3139, CATH Superfamily 2.60.40.740 or RIII: IPR013783 [Pfam: PF01345, DUF11]), and a membrane-spanning sequence at its C terminus (RIV) (Fig. 1.4). The arrangement of the signal sequence and the single membrane-spanning sequence suggest that the product of MTCT_1020 is a membrane-bound protein at its C-terminal domain with a large middle region located outside of the membrane. In CLA160, most of the middle domain and the membrane-spanning sequence are absent from the product of MTCT_1020 due to its nonsense mutation (Table 1.1). Therefore, it is possible that the large middle region is involved in aggregation in CaT2. The middle region of MTCT_1020 is composed of two different portions: the first repeated region (RII) and second repeated region (RIII) (Fig. 1.4). RIII contains 11

repeated domains of DUF11 (Pfam: PF01345). However, a domain search analysis using hmmsearch with the hmm model of DUF11 against the database, restricted to *Methanothermobacter* (taxid: 145260) (Table 1.3) indicated that *Methanothermobacter* species possess proteins, such as MTCT_0976 of CaT2, MTH_1074 of *Methanothermobacter thermautotrophicus* ΔH, and MTBMA_c14630 of *M. marburgensis* (Fig. 1.4). These proteins are uncharacterized, and in contrast to CaT2, *M. thermautotrophicus* ΔH and *M. marburgensis* do not aggregate (Kosaka T. *et al*., 2014). Furthermore, another DUF11 domain-containing protein (MTCT_P1_0005) was found in CaT2 by this search, which was not mutated in CLA160 (Fig. 1.4). These results suggest that the RIII DUF11 domain-repeated region of MTCT_1020 is not important for aggregation, whereas RII, containing conserved repeated domains or the whole structure, may be responsible for the function of MTCT_1020 in the aggregation of CaT2. Notably, the conserved domains in RII (FunFam 3139: CATH Superfamily 2.60.40.740) showed gene ontology (GO) terms such as calcium ion binding (GO:0005509), metal ion binding (GO:0046872), and extrachromosomal circular DNA (eDNA) (GO:0005727), suggesting that other materials, metal ions, and eDNA are involved in the aggregation of CaT2.

A DELTA search for MTCT_1020 against the non-redundant (nr) database in NCBI indicated that proteins homologous to that encoded by MTCT_1020 are distributed not only in methanogens, but also in bacteria (Fig. 1.5). *M. formicicum* and *M. smithii* showed the aggregation phenotype (Bang *et al.*, 2014; Wu *et al*., 1992) and were previously reported to aggregate in dense granules in methanogenic reactors (Wu *et al*., 1992) or microflora (Samuel *et al*., 2007), respectively. This result supports the contribution of MTCT_1020 to aggregation and suggests an aggregating capability in the listed strains by their MTCT_1020-homologous proteins.

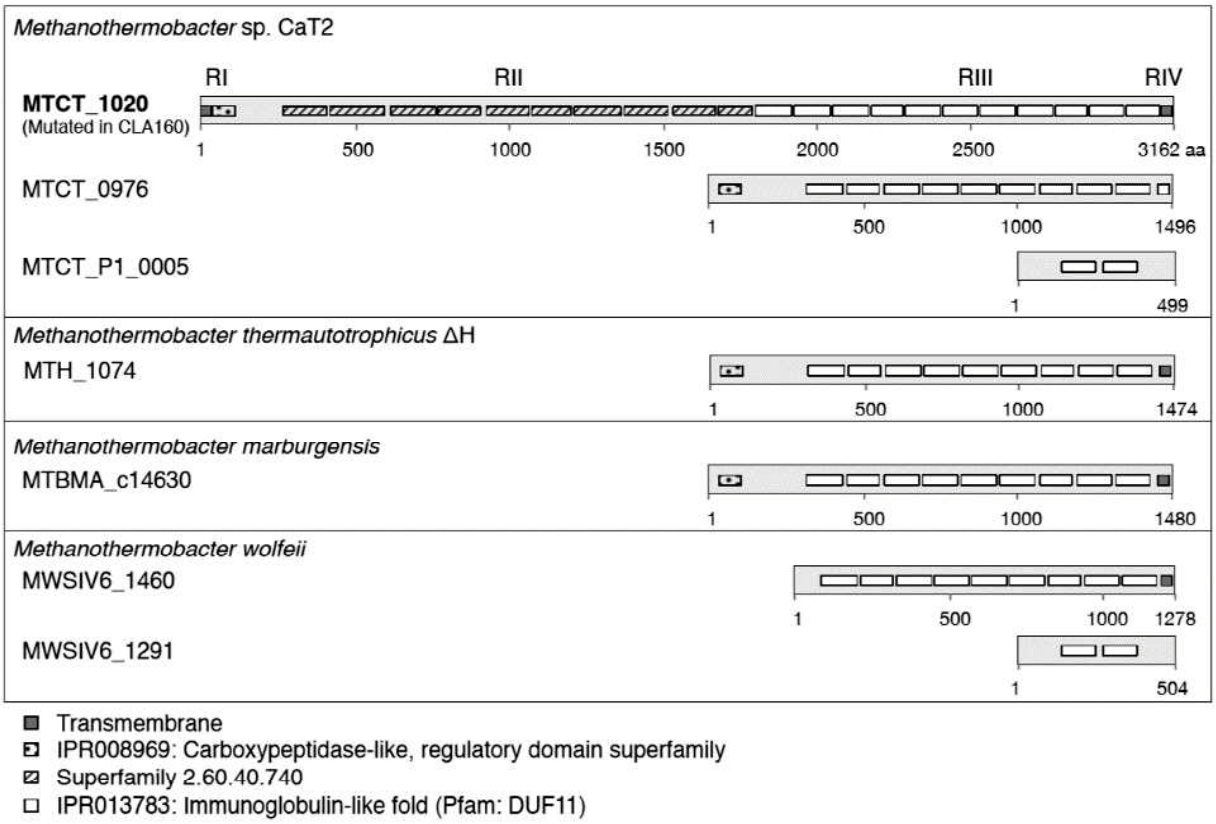

Fig. 1.4 Predicted domain architecture of MTCT_1020 (T2GKU7, the mutated gene of CLA160), MTCT_0976 (T2GJL3), and MTCT_P1_0005 (T2GLL5) (CaT2), MTH_1074 (O27146) (ΔH), MTBMA_c14630 (D9PXU4) (*marburgensis*)

All datasets were obtained from Uniprot database (http://www.uniprot.org), including InterPro (https://www.ebi.ac.uk/interpro). The numbers depicted under each box are amino acid number.

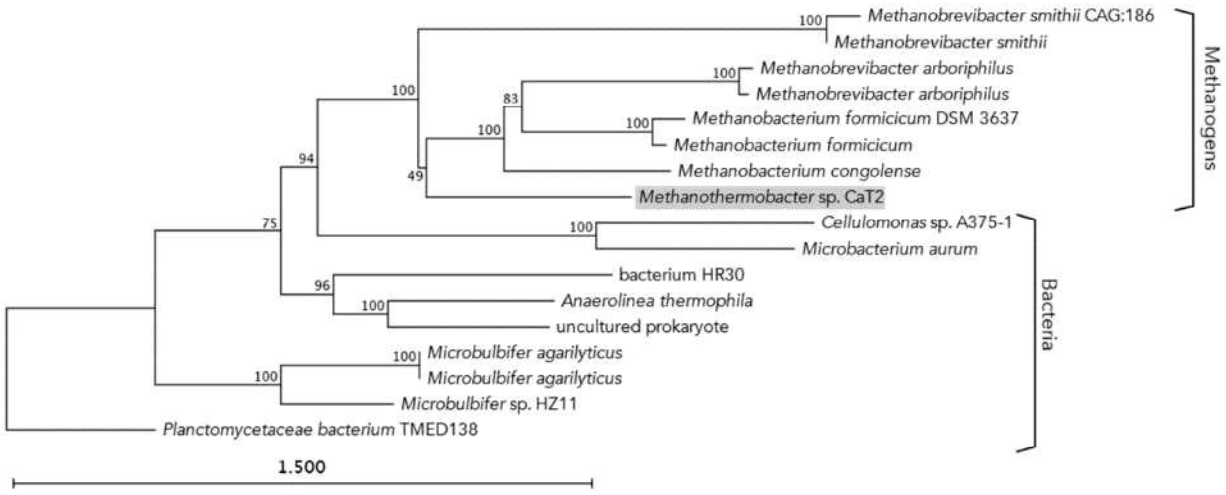

Fig. 1.5 Phylogeny of *MTCT_1020*-encoded protein and its homologues

A multiple sequence alignment of the amino acid sequences of the *MTCT_1020*-encoded protein and the homologous proteins of *Methanothermobacter* sp. CaT2 (WP_084126234.1: accession number), *Methanobacterium congolense* (WP_084789945.1), *Methanobacterium* sp. MO-MB1 (WP_100905616.1), *Methanobrevibacter arboriphilus* (WP_080459654.1), *Methanobrevibacter arboriphilus* (WP_042702822.1), *Methanobacterium formicicum* DSM 3637 (EKF85388.1), *Methanobacterium formicicum* (WP_082055701.1), *Methanobrevibacter smithii* (WP_019262854.1), bacterium HR30 (GBD25567.1), *Planctomycetaceae bacterium* TMED138 (OUV71746.1), uncultured prokaryote (BAL57189.1), *Anaerolinea thermophila* (WP_013559229.1), *Methanobrevibacter smithii* CAG:186 (CDF29159.1), *Microbulbifer* sp. HZ11 (WP_043320659.1), *Microbulbifer agarilyticus* (AQQ68885.1), *Microbulbifer agarilyticus* (WP_077407055.1), *Microbacterium aurum* (WP_076691662.1) and *Cellulomonas* sp. A375-1 (WP_048344453.1) was generated using ClustalO with default parameters and the consequent phylogenetic tree was generated using the Create Tree tool program with the neighbor-joining method (the Kimura correction) and 1,000 bootstrap replications in CLC Sequence Viewer 8.0 (http://www.clcbio.com). The scale bar corresponds to 0.1 substitution per amino acid.

Table 1.3 The hmmsearch using DUF17 model against *Methanothermobacter* protein sequences in Uniprot database

Strains	Aggregation	Uniprot No.	Protein	Locus_tag	Length	E-value*
Methanothermobacter sp. CaT2	+	T2GKU7	Uncharacterized protein	MTCT_1020	3,1621	8E-217
		T2GJL3	Uncharacterized protein	MTCT_0976	1,4964	1E-182
		T2GLL5	Uncharacterized protein	MTCT_P1_0005	499	1.6E-18
Methanothermobacter thermautotrophicus ΔH	-	O27146	Putative membrane protein	MTH_1074	1,4742	4E-188
Methanothermobacter marburgensis Marburg	-	D9PXU4	Uncharacterized protein	MTBMA_c14630	1,4803	3E-177
Methanothermobacter wolfeii	?	A0A1M4MTN5	Uncharacterized protein	MWSIV6_1460	1,2785	7E-163
		A0A1M4MT64	Uncharacterized protein	MWSIV6_1291	504	5.8E-17
Methanothermobacter sp. EMTCatA1	?	A0A223YY22	Uncharacterized protein	tca_01038	1,4752	1E-180

*The search threshold was <1E-10.

1.3.5 Effects of DNase I and metal ions on the aggregation of CaT2

Previous findings suggested that eDNA and metal ions are involved in the aggregation mechanisms of CaT2. eDNA and metal ions have been shown to play a role in the cell-to-cell interactions of microorganisms (Orell *et al*., 2013; Schmidt *et al*., 1993). To elucidate the mechanisms underlying aggregation in more detail, sedimentation experiments on CaT2 and CLA160 were performed following their treatment with DNase I or the addition of the metal ions Ca^{2+} and Mg^{2+}. The DNase I treatment had almost no effect on the sedimentation indices of CaT2 and CLA160 (Fig. 1.6 A). Conversely, the addition of $CaCl_2$ reduced the sedimentation index of CaT2, but not of CLA160 (Fig. 1.6 B). The addition of $MgCl_2$ had a similar effect to that of Ca^{2+} ions on CaT2 (Fig. 1.6 B). These results suggest that Ca^{2+} or Mg^{2+} ions enhance the aggregation of CaT2.

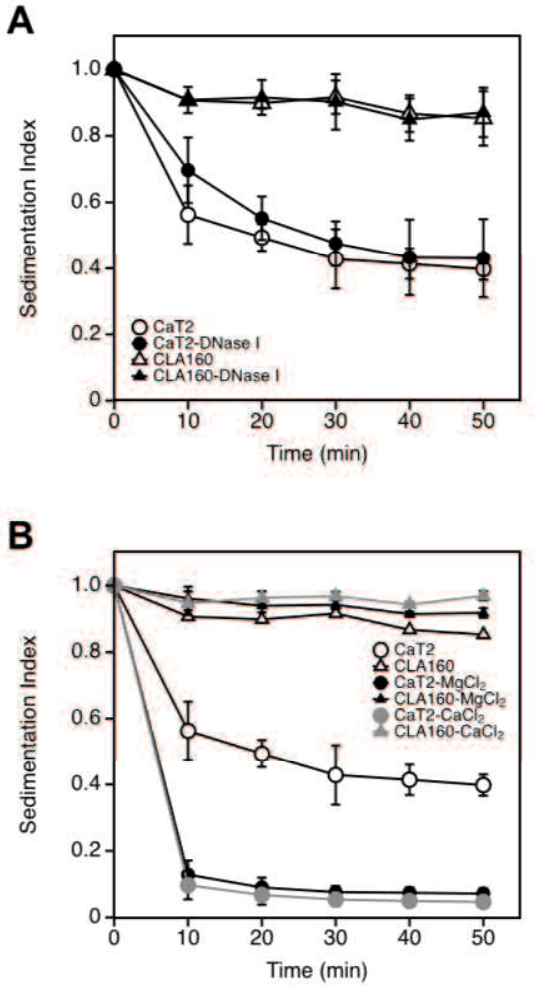

Fig. 1.6 Effects of the DNase treatment or addition of metal ions on sedimentation indices of CaT2 and CLA160. (A) CaT2 (circles) and the aggregation-defective mutant CLA160 (triangles) were treated with DNase I (closed) or untreated (open) and then subjected to a sedimentation analysis. (B) CaT2 (circles) and the aggregation-defective mutant CLA160 (triangles) were treated with $CaCl_2$ or $MgCl_2$. Error bars represent standard deviations of the means of three independent experiments.

1.4 DISCUSSION

In the present study, we isolated the aggregation-defective mutant, CLA160, from *Methanothermobacter* sp. CaT2, which normally forms aggregated clumps via tight cell-to-cell interactions (Fig. 1.1). Although it has been proposed that the cell-to-cell interactions of CaT2 are mediated by a surface sugar layer (Kosaka *et al*., 2013), TEM observations suggest that CLA160 retains a surface sugar layer that is thinner than that of CaT2 (Table 1.2). Seven genes have been predicted to be responsible for aggregation in CaT2 (Kosaka *et al*., 2014); however, there were no mutations in these genes in CLA160, and the remaining mutations in CLA160 were located in the non-coding regions of its genome (Table 1.1). The proteinase K treatment and a genomic analysis of CLA160 showed that MTCT_1020, which encodes a putative extracellularly protruding membrane protein, plays a role in the dense aggregation properties of CaT2. Since protein-mediated cell-to-cell adhesion may be observed in many microorganisms (Alsteens *et al*, 2013; Bodelón *et al*., 2013; El-Kirat-Chatel *et al*., 2015; Miki *et al*., 1982), protein-mediated aggregation is not unexpected. We presume that MTCT_1020 is a protein that contributes not only to aggregation, but also to the stabilization of the surface sugar layer. However, a low level of aggregation was observed morphologically in CLA160 (Fig. 1.1 B), while no obvious proteinase K effect was observed in this strain (Fig. 1.3), suggesting that another mechanism, other than a protein-mediated one, is involved in the aggregation of CaT2. One possibility is the sugar layer, which remains present in CLA160 (Fig. 1.1 H).

The protein encoded by MTCT_1020 showed a specific sequence structure, with its signal sequence and single membrane-spanning sequence suggesting that this protein is membrane-anchored at its C-terminal domain and its RII is important for cell-to-cell interactions (Fig. 1.4). This RII portion may be related to adhesion and the metal ion binding region, which is supported by a Conserved Domain Search

(https://www.ncbi.nlm.nih.gov/Structure/cdd/wrpsb.cgi), identifying it as a D2 domain. This D2 domain consists of the repetition of the major component RrgB, which is also the main component that forms the backbone in Pneumococcal pili (Spraggon *et al*., 2010). Therefore, these regions may bind with each other. Although our prediction suggests that RIII containing the repeated DUF11 domain is not responsible for aggregation, DUF11 is often found in membrane proteins in a small number of phylogenetically distant prokaryotes. In the MTCT_1020 encoded protein, each of the DUF11 repeat sequences overlapped with sequences of five to 10 motifs of 11 DUF11 domains consisting of 120-residue repeats. DUF11-containing repeat domains are not associated with aggregation, but may be important for stabilizing the surface cell wall structures of MTCT_1020.

Ca^{2+} or Mg^{2+} ions enhance the aggregation of CaT2, but not that of CLA160 (Fig. 1.6 B). This result prompted us to speculate that metal ions stimulate cell-to-cell interactions via a direct association with the MTCT_1020-encoded protein. The enhancement of cell flocculation by metal ions has been reported for several microorganisms (Salehizadeh *et al*., 2001; Shahadat *et al*., 2015; Wang *et al*., 2006). In the halo-tolerant archaea *Halobacterium salinarum*, Ca^{2+} ions were found to be essential for initiating cell aggregation, while Mg^{2+} ions did not induce the flocculation of cells (Kawakami *et al*., 2007). The pathogenic, Gram-negative, auto-aggregating bacterium Legionella pneumophila exerted a metal ion enhancement effect on an auto-aggregation process, which is mediated by the Legionella collagen-like protein in a divalent cationdependent manner (Abdel-Nour *et al*., 2014). Moreover, in the eukaryote Saccharomyces cerevisiae, Ca^{2+}-dependent, lectin-like interactions were found between proteins related to flocculation and specific sugar residues on the surfaces of other cells (Kobayashi *et al*., 1998; Verstrepen *et al*., 2004). Therefore, aggregation enhancement mechanisms by proteins and cationic ions are common and widespread among microorganisms. Interestingly, the enhancement of start-up granulation by the addition of Ca^{2+} ions has also been reported in UASB

reactors (Chong *et al.*, 2012; Pevere *et al*., 2007; Tiwari *et al*., 2007). The functions of proteins homologous to that encoded by MTCT_1020 are mostly unknown (Fig. 1.5). An investigation into the relationships between MTCT_1020 and metal ions and their influence on aggregation may enhance current knowledge on the aggregating mechanisms of methanogens and may also supply new information about other aggregating microorganisms. Finally, our results suggest that an extracellular protein that possesses repeated sequences and a unique structure is a core factor in the aggregation of *Methanothermobacter* sp. CaT2.

CHAPTER 2

Characteristics of physiology of and genomic mutations in aggregation-enhanced mutants of *Methanothermobacter* sp. CaT2

ABSTRACT

The thermophilic hydrogenotrophic methanogen *Methanothermobacter* sp. CaT2 aggregates by itself. CaT2 is known to have a surface sugar layer and extracellular proteins that may be related to its aggregation. Aggregation-enhanced mutants, CHA001 and CHA002, were isolated after repeated cultivation for more than two years. When treated with proteinase K, CHA001 and CaT2 similarly exhibited a very low degree of aggregation and CHA002 exhibited less aggregation but still retained aggregation, suggesting protein-based aggregation via extracellular proteins in both CHA001 and CHA002, presumably via a putative membrane-bound and extracellularly protruding protein, MTCT_1020, identified previously. Genomic analysis revealed that CHA001 and CHA002 shared a missense mutation of MTCT_1348 and had distinct mutations. These results suggested that the MTCT_1348 mutation provides subsidiary support to the adhesive function of extracellular proteins and that there is an additional mutation(s) in CHA002 for the non-proteinous aggregation capability.

2.1 INTRODUCTION

Methane is produced under either mesophilic or thermophilic conditions in bioreactors, generally in upflow anaerobic sludge blanket (UASB) reactors (Uemura S. and H. Hrada, 1993; Schmidt *et al*., 1995). The fermentation efficiency of a UASB reactor depends on the activity of granules that have been formed (Schmidt *et al*., 1996; Liu *et al*., 2003). The granules are composed of many kinds of microorganisms including primary fermenting bacteria, secondary fermenting bacteria, acetoclastic methanogens and hydrogenotrophic methanogens (Schmidt *et al*., 1996; Satoh *et al*., 2007; Liu *et al*., 2002; Sekiguchi *et al*., 1999). Of these, methanogens appear to be crucial species for granule formation (Uemura S. and H. Hrada, 1993; Zinder *et al*., 1984; Fernández *et al*., 2008,). The granule environment in thermophilic reactors allows methanogens to produce a 2-3-times larger amount of methane than that in mesophilic reactors (Orell *et al*., 2013; Harada *et al*., 2004). However, granule formation is generally more difficult in thermophilic reactors than in mesophilic reactors (Harada *et al*., 2004). The difficulty of granule formation in thermophilic reactors may be due to the difference in aggregation mechanisms including responsible molecules under mesophilic and thermophilic conditions. Therefore, elucidation of the mechanisms by which thermophilic methanogens aggregate is an attractive issue for the stabilization of fermentation in UASB reactors.

Aggregation formation in many microorganisms is known to be established via various substances including extracellular DNA (eDNA), proteins, lipids and polysaccharides (Liu *et al*., 2003; Orell *et al*., 2013; Flemming *et al*., 2010; Liu *et al*., 2004; Veiga *et al*., 1997). The substances and mechanisms for the aggregation of several mesophilic methanogens have been reported. *Methanosarcina mazei* forms polysaccharide-based extracellular polymers that attach to the outer surfaces of cells (Robinson *et al*., 1985). *Methanobacterium formicicum* and *Methanobrevibacter* sp. produce extracellular polymers (ECPs) to spatially connected between

aggregates formed by other species (Schmidt *et al*., 1996; Veiga *et al*., 1997). *Methanococcus maripaludis* adheres to the surface of other microbes via flagella and pili (Jarrell *et al*., 2011). However, studies on the aggregation of thermophilic methanogens have been limited. In the case of the thermophilic aggregating hydrogenotrophic methanogen *Methanothermobacter* sp. CaT2, its cell-surface sugar layer has been assumed to be responsible for its aggregation properties on the basis of physiological analysis (Kosaka *et al*., 2014). Comparative genomic analysis with other thermophilic hydrogenotrophic methanogens revealed that CaT2 has specific aggregation-related adhesion genes but pili (fimbriae) cause no strong cell-cell interaction of CaT2 (Kosaka *et al*., 2013; Kosaka *et al*., 2014). Recently, the analysis of an aggregation-defective mutant has strongly suggested that MTCT_1020 is involved in the aggregation of CaT2 (Sumikawa *et al*., 2019). However, it is not clear whether the cell-surface sugar or specific aggregation-related adhesion proteins are involved in the aggregation formation in addition to MTCT_1020.

In order to clarify the detailed molecular mechanisms underlying cell-cell interaction of CaT2, we isolated two mutants, CHA001 and CHA002, that exhibited significantly enhanced aggregation. Both mutants were characterized by morphological analyses, proteinase K and DNase I treatments, and methane production experiments. These phenotypic characterizations and genomic analysis of CHA001 and CHA002 revealed new aspects of the aggregation mechanism of CaT2.

2.2 MATERIAL AND METHODS

2.2.1 Strains and growth conditions

Methanothermobacter sp. CaT2 (DSM 24414 and NBRC 107770) and its mutant derivatives were used in this study. Strains were grown in W medium at 55°C as previously described (Kosaka *et al*., 2014), or in W-R medium (W medium without resazurin solution) under a controlled atmosphere: 160 kPa H_2/CO_2 (80/20, v/v) (Sumitomoseiki, Osaka, Japan).

The aggregation-enhanced mutants CHA001 and CHA002 were isolated as follows. CaT2 was repeatedly cultivated in W medium at 55°C for over two years and then the culture was diluted and spread on W medium gellan gum plates (Nakamura *et al*., 2011) to form colonies. About 200 colonies were individually cultivated in W medium under H_2/CO_2 (80/20, v/v) to observe aggregation under a microscope. After conducting the aggregation experiments several times, cells that showed strong aggregation were selected as an aggregation-enhanced mutant. The phenotype was confirmed under a phase-contrast microscope (Eclipse E600; Nikon, Tokyo, Japan). Aggregation size in phase contrast images was measured using the polygon selection and measure function in ImageJ software (Schneider C.A. *et al*., 2012).

2.2.2 Observation under a phase-contrast, scanning electron microscope (SEM) and a transmission electron microscope (TEM)

Sample preparation for observation by an SEM and a TEM was carried out as described previously (Sumikawa *et al*., 2019). A fluorescence microscope (Eclipse E600; Nikon, Tokyo, Japan) was used to take phase-contrast images. SEM images were taken using the following procedure. Cell pellets were fixed for 3 h with 1.25% glutaraldehyde in 0.1 M cacodylate buffer (pH 6.5) at 4 °C, washed with 0.1 M cacodylate buffer, and then suspended with a small amount of the same buffer. The suspension was dropped on a 0.2 μm cellulose membrane filter and dehydrated with a graded ethanol series and t-butylalchol. The dehydrated filter was dried using

vacuum freeze-drying equipment (VFD-21S; Vacuum Device, Ibaraki, Japan). The dried membrane filter was then coated with platinum (Auto Fine Coater, JFC-1600; JEOL, Tokyo, Japan). Images of sections were obtained by observation using an SEM (10 kV, 30 μs; JSM-6360LA; JEOL, Tokyo, Japan). Observation by a TEM with ruthenium red was performed as previously described (Kosaka *et al*., 2014), with slight modifications. Cell pellets were fixed for 5 h with 1.25% glutaraldehyde and 0.5 mg/ml ruthenium red in 0.1 M cacodylate buffer (pH 6.5) at 4 °C, washed in 0.1 M cacodylate buffer, and post-fixed for 2 h in 1% osmium tetroxide containing 0.5 mg/ml ruthenium red in 0.1 M cacodylate buffer at 4°C. After being rinsed with 0.1 M cacodylate buffer, the pellets were embedded in a 3% agarose gel and dehydrated with a graded ethanol and acetone series. The dehydrated blocks were embedded in Epok 812 (Kohken, Tokyo, Japan). Ultra-thin sections were cut using a diamond knife mounted in an ultramicrotome (EM-UC6; Leica, Wetzlar, Germany) and then placed on copper grids and stained with uranyl acetate and lead citrate. TEM examination was performed using a Tecnai G2 Spirit electron microscope (Thermo Fisher Scientific, Massachusetts, USA) at an acceleration voltage of 80 kV.

2.2.3 Gas-phase analysis

Methane and hydrogen were analyzed using a gas chromatography system (GC-8A and C-R6A; Shimadzu, Kyoto, Japan) with a thermal conductivity detector and a column (2 m × 3 mm stainless steel) packed with Unibeads C 60-80 (GL Science, Tokyo, Japan). The analysis conditions were as follows: injection at 150 °C, column at 145 °C, detector at 150°C, current for the detector at 50 mA, and flow rate of carrier Ar gas at 30 mL/min.

2.2.4 Sedimentation index assay with various treatments

Cell growth and sample treatments for a sedimentation index assay were carried out as described previously (Sumikawa *et al*., 2019). Cells were grown in W-R medium at 55°C for 4

days under H_2/CO_2 (80/20, v/v), recovered by centrifugation, washed twice, and suspended in 10 mM Tris-HCl buffer (pH 7). The suspensions were subjected to optical density measurement or to the following treatments: proteinase K treatment, DNase I treatment and addition of $CaCl_2$, which were carried out as described previously (Sumikawa *et al*., 2019). For proteinase K treatment, proteinase K (Wako Pure Chemical Industries, Ltd., Osaka, Japan) was added to the cell suspension at a final concentration of 10 μg/mL and the solution was incubated for 1 h at 37 °C. A control examination was performed by the addition of 10 mM Tris-HCl buffer instead of proteinase K. After incubation, cells were washed once with 1 mL of 10 mM Tris-HCl buffer and subjected to a sedimentation index assay. For DNase I treatment and addition of $CaCl_2$, DNase I, $CaCl_2$, and Tris-HCl buffer were added to cell suspensions at final concentrations of 5 μg/mL, 10 mM, and 10 mM, respectively, and the solutions were incubated for 1 h at 37 °C. A control examination was performed by the addition of 10 mM Tris-HCl buffer instead of DNase I or $CaCl_2$. After incubation, the cells were washed once and suspended in 10 mM Tris-HCl buffer. To compare the speeds of sedimentation of the cells, the cell suspensions were mixed briefly and their values of turbidity were measured at OD_{600} every 10 mins for 50 min using a photometer (Libra S12; Berthold Technologies, Bad Wildbad, Germany). The sedimentation index was calculated using the following equation: Sedimentation index = (value of turbidity at each measured time) / (value of turbidity at 0 min) × 100.

2.2.5 Extraction of genomic DNA

Cell growth and genomic DNA preparation were carried out as described previously (Sumikawa *et al*., 2019). Cells were grown in 500 mL of W medium at 55°C for 4 days under H_2/CO_2 (80/20, v/v), recovered by centrifugation (12,000 rpm) at 4°C for 15 min, and washed twice with dH_2O. Cell pellets were suspended in TE buffer. The suspension was then subjected to a 5-times freeze-thaw treatment with freezing at −80°C for 30 min and thawing at 55°C for 10

min. The treated solutions were incubated overnight at 55°C following the addition of SDS, proteinase K, NaCl, and RNase A at final concentrations of 0.5% (w/v), 100 μg/mL, 10 mM, and 10 μg/mL, respectively. After incubation, each solution was gently mixed by inversion with double the volume of TE-saturated phenol. A half-volume of chloroform was added, and the solution was kept on ice for 5 min before being centrifuged at 14,000 rpm for 15 min at 4 °C. Sodium acetate (pH 8) was then added to the transferred upper aqueous layer to a final concentration of 0.3 M. The solution was gently mixed with an equal volume of isopropanol and centrifuged at 14,000 rpm for 15 min at 4°C. The precipitate was washed with an equal volume of 70% (v/v) ethanol and centrifuged at 14,000 rpm for 15 min at 4°C. The resultant precipitate was dried and resuspended in 100 μL of TE buffer. The sample of genomic DNA was further purified using a Genomic-tip 20 kit (Qiagen, Hilden, Germany) according to the manufacturer's instructions.

2.2.6 Genome sequencing and mapping analysis of CHA001 and CHA002 strains against CaT2 genome sequences

Five micrograms of genomic DNA of CHA001 and CHA002 dissolved in Tris-EDTA buffer was digested by a Covaris S-2 sonicator (Covaris, Woburn, MA, USA) with an average size of 500 bases. Construction of a DNA library and sequencing with 300 base by a massively parallel sequencer (MiSeq; Illumina KK, Tokyo, Japan) was followed as the previous study (Akuzawa S. *et al*., 2016). The sequenced reads were screened by a quality score higher than the Phred score 30 and were trimmed 12 bases from the 5' end and 20 bases from the 3' ends. The truncated reads less than 150 base or with ambiguous nucleotides was removed from further analysis. We previously reported the complete genome sequence for *Methanothermobacter* sp. CaT2, which is available at DDBJ/EMBL/GenBank, accession numbers AP011952.1 and AP011953.1 (Kosaka *et al*., 2013). Mutation sites were searched by read mapping using CLC Genomics Workbench version 7.5 (Qiagen, Venlo, Netherland) with following parameters; match

score: 1; mismatch cost: 2; Insertion/deletion cost: 3; length fraction: 0.7; similarity fraction: 0.9. The filter settings for SNP and In-del calling was followed as previous study (Hirokawa *et al*., 2018).

2.2.7 Sequence data deposition

Illumina sequence reads of the CHA001 and CHA002 strains have been deposited in the DDBJ Sequence Read Archive. The BioSample accession numbers of CHA001 and CHA002 are SAMD00184547 and SAMD00184548, respectively.

2.3 RESULTS

2.3.1 Characterization of the aggregation-enhanced mutants CHA001 and CHA002

Methanothermobacter sp. CaT2 with an intrinsic aggregation ability was repeatedly cultivated for over two years, from which aggregation-enhanced mutants, CHA001 and CHA002, were obtained. Morphologies of the mutants were observed under a phase-contrast microscope, a scanning electron microscope (SEM) and a transmission electron microscope (TEM). Phase-contrast and SEM analyses revealed that CHA001 and CHA002 formed larger and denser aggregates than those formed by CaT2 (Fig. 2.1 A-F) and that the size of aggregates of CHA002 were larger than that of aggregates of CHA001 (Fig. 2.2). In addition, the aggregation size of CHA001 was larger than that of CaT2 (Fig. 2.2). Moreover, SEM analysis revealed that the two mutants exhibited similar smooth cell-surface structures (Fig. 2.1 E, F). TEM analysis with sugar-staining samples revealed that the thicknesses of surface sugar layer of CHA001 and CHA002 were similar to that of CaT2 or slightly thinner, respectively, and that the thicknesses of cell wall of CHA001 and CHA002 were slightly thinner or thinner than that of CaT2,

respectively (Fig. 2.1 G-I and Table 2.1). On the basis of these findings, it is likely that the order of aggregation strength is CHA002, CHA001, and CaT2, which is consistent with their aggregation indices (see below), and that the mutations of both mutants have no effect on the surface sugar layer.

In order to examine the relationship between aggregation strength and methane productivity, the mutants and CaT2 were cultured with hydrogen as a substrate under a shaking condition (Fig. 2.3), which led to dispersal of large aggregates. The amount of methane produced by CHA001 was almost the same as that produced by CaT2. On the other hand, CHA002 produced methane at an early exponential phase compared to CaT2. It is thus assumed that CHA002 can perform efficient metabolism via its stronger cell-cell interaction that is sufficient to some extent even under a shaking condition.

Table 2.1 Thicknesses of the cell wall (CW) and sugar layer (SL) in aggregation-enhanced mutants CHA001 and CHA002

Strain	CW[a]	SL[a]
CHA001	11.8 ± 1.5	13.6 ± 0.9
CHA002	6.8 ± 1.1	9.1 ± 1.4
CaT2[b]	15.2± 1.3	12.7±0.8

[a]The thickness of the layer structure was measured from each TEM image. Standard deviations are indicated after the measurements (n = 7).

[b]Data from Sumikawa *et al*., 2019.

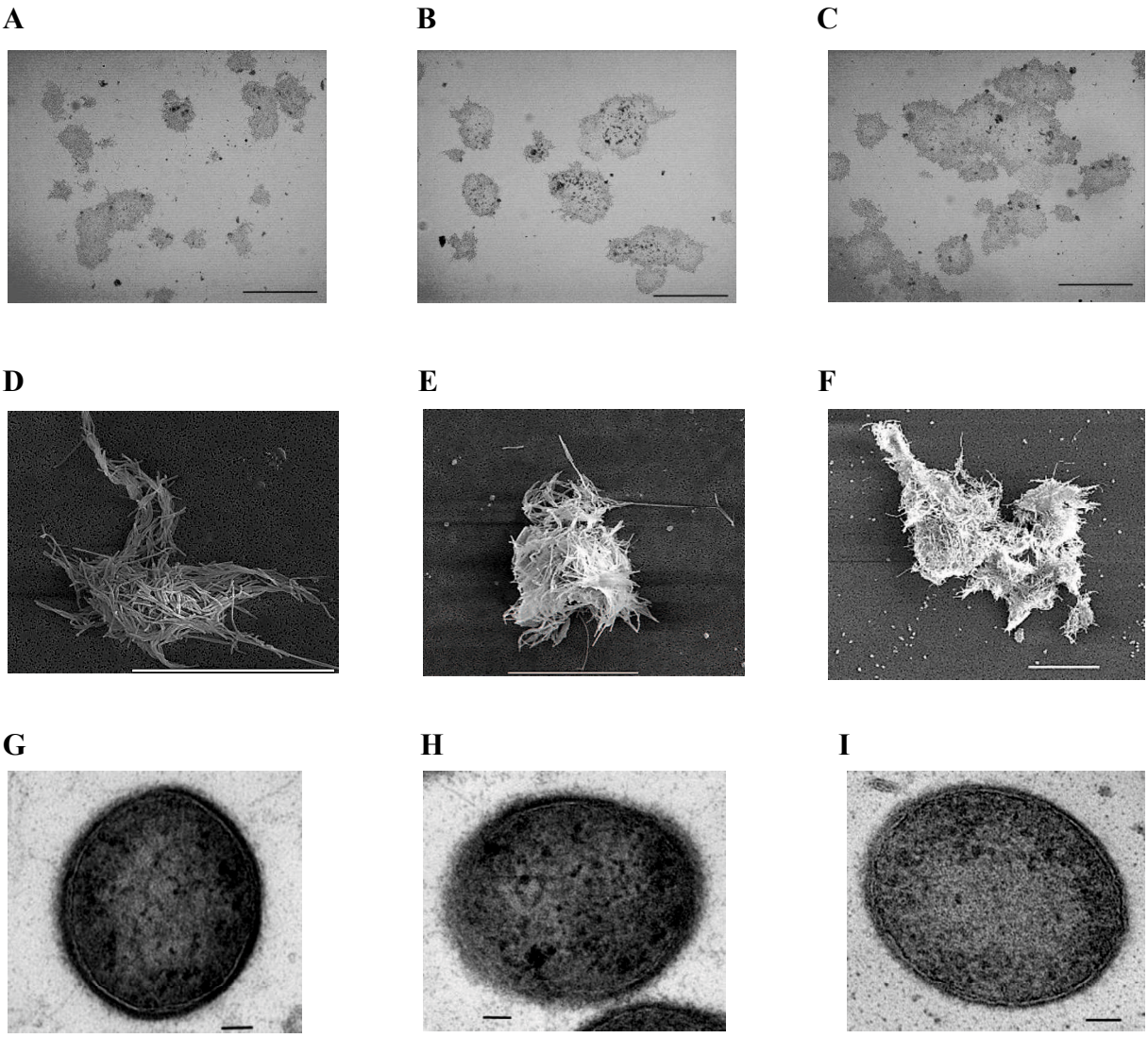

Fig. 2.1 Images of Methanothermobacter sp. CaT2 and the aggregation-enhanced mutants, CHA001 and CHA002

Phase-contrast images of CaT2 (A), CHA001 (B) and CHA002 (C) were taken at 100× magnification. SEM images of CaT2 (D), CHA001 (E) and CHA002 (F) were taken at 6,000×, 4,000× and 1,600× magnifications, respectively. TEM images of CaT2 (G), CHA001 (H) and CHA002 (I). Bars represent 200 μm in A, B and C, 30 μm in D, E and F, 50 nm in G, I and H.

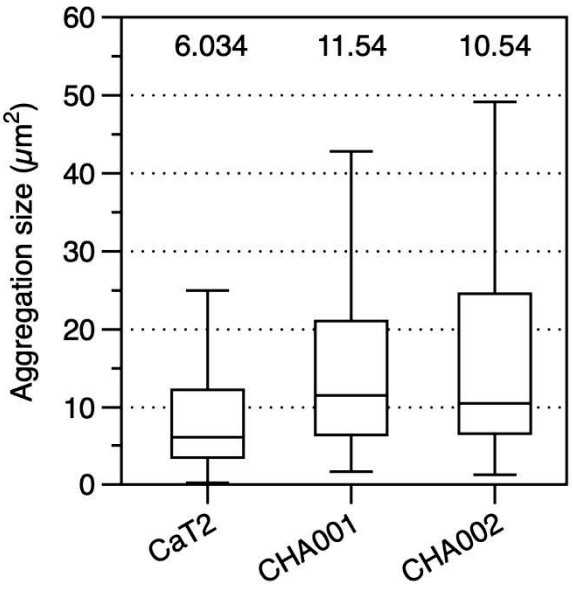

Fig. 2.2 Aggregation size of CaT2, CHA001, and CHA002

Box plot of the aggregation size (area: μm^2) of CaT2 and aggregation-enhanced mutants, CHA001 and CHA002. The size of >200 aggregations were estimated with 100× phase contrast microscopy using ImageJ. The values shown are the median of each sample. The outlier, a value that is >1.5× of the Inner Quartile Range from the median calculated in the Datagraph software, was eliminated.

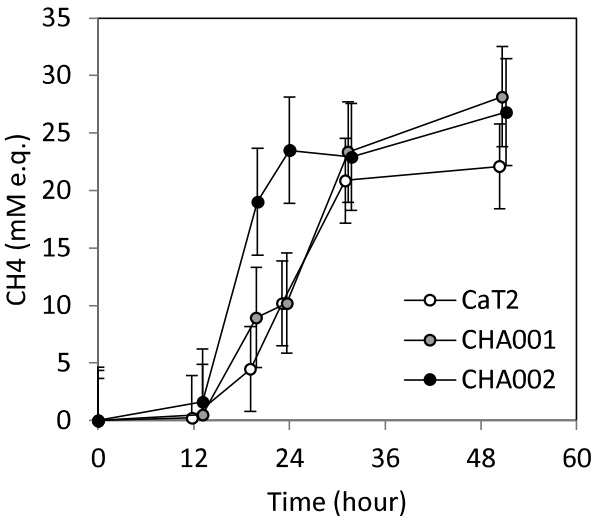

Fig. 2.3 Comparison of methane production by CaT2, CHA001, and CHA002

CaT2 (open circles) and aggregation-enhanced mutants CHA001 (gray circles) and CHA002 (black circles) were grown in W medium under H_2/CO_2 (80/20, v/v) and methane production was measured. Error bars represent standard deviations of the means of three independent experiments.

2.3.2 Aggregation of CHA001 and CHA002 mediated by extracellular proteins

To evaluate the aggregation capability, experiments for determining the sedimentation index of cells were performed as described previously (Kosaka *et al*., 2014). The indices of CHA001 and CHA002 were similar to those of CaT2 (Fig. 2.4 and 2.5), suggesting that the enhancement of aggregation of mutants compared with that of CaT2 were difficult to distinguish on sedimentation indices.

The results of proteinase K treatment in a previous study suggested that CaT2 has extracellular proteins responsible for its aggregation (Sumikawa *et al.*, 2019). Proteinase K treatment was thus performed for CHA001 and CHA002 to examine whether extracellular proteins are involved in their aggregations. CHA001 showed a large decrease in sedimentation as did CaT2 after the proteinase K treatment (Fig. 2.4 A). CHA002 also showed a decrease in sedimentation but still sedimented to some extent compared to that of CaT2 even after proteinase K treatment (Fig. 2.5 A). These findings suggest that CHA002 possesses a strong aggregation capability followed by CHA001 and then CaT2 and that CHA002 has an additional aggregation factor(s) in addition to the proteinous factors.

2.3.3 Effects of DNase I and metal ions on aggregation of CHA001 and CHA002

The aggregation of CaT2 was not influenced by treatment with DNase I but was strengthened by the addition of Ca^{2+} (Sumikawa *et al.*, 2019). We thus examined the effects of treatment with DNase I and addition of $CaCl_2$ on the sedimentation of CHA001 and CHA002 cells. DNase I treatment had almost no effect on the sedimentation of CHA001 or CHA002 cells (Fig. 2.4 B and 2.5 B), suggesting that eDNA is not engaged in the aggregation of either mutant. On the other hand, the addition of $CaCl_2$ slightly increased the sedimentation of CHA001 and CHA002 as in the case of CaT2 (Fig. 2.4 c and 2.5 c). These results suggest that Ca^{2+} ions enhance the aggregation of both CHA001 and CHA002 as well as CaT2.

2.3.4 Genomic analysis of mutations in CHA001 and CHA002

CaT2 bears an extracellular protein *MTCT_1020* that is responsible for its aggregation (Sumikawa *et al.*, 2019). CHA001 and CHA002 as derivatives of CaT2 exhibited enhanced aggregation and were thus expected to have mutations. Genomic sequencing was performed to identify the mutations in CHA001 and CHA002. Both mutants were found to have no mutation in *MTCT1020*. On the other hand, there were mutations in two genes and three genes in CHA001 and CHA002, respectively, in addition to a deletion mutation in the non-coding region in both mutants (Table 2.2). Of these, two mutations were shared by the mutants. One of the two mutations was an amino acid substitution mutation in *MTCT_1348*, which encodes a pyridoxamine 5'-phosphate oxidase. In CHA001, there was an additional mutation causing an amino acid substitution in *MTCT_0393*, which encodes the ATP-binding subunit, consisting of 480 amino acid residues, of a cobalt transporter. The mutation in *MTCT_0393* was a nonsense mutation, resulting in a reduction in the size of the product to 8 amino acid residues. In CHA002, there was an additional mutation causing an amino acid substitution in *MTCT_0179* for acetate-CoA synthetase with 635 amino acid residues. The mutation in *MTCT_0179* was a nonsense mutation, resulting in a small product with 72 amino acid residues. The other mutation in CHA002 was in *MTCT_0445* for a DUF2085 domain-containing protein with 111 amino acid residues. The mutation in *MTCT_0445* was a frame-shift mutation causing a small product with 50 amino acid residues. The other mutations in both mutants were found in a non-coding region.

Table 2.2 Summary of mutations in CHA001 and CHA002

Position	Gene	Product	Mutation	Amino acid substitution	Amino acid number	CHA001	CHA002
1323438	*MTCT_1348*	Pyridox-amine 5'-phosph-ate oxidase	Nucleotide substitution T → C	Thr189Ala	313	+	+
354842	*MTCT_0393*	Cobalt ABC transporter ATP-binding subunit	Nonsence mutation TG → T	Val9Stop	480 to 8	+	—
146492	*MTCT_0179*	Acetyl-CoA synthetase	Nonsence mutation AG → A	Val73Stop	635 to 72	—	+
436706	*MTCT_0445*	DUF2085 domain-containing protein	Insertion AAC → ACCAC	Asn13 Frame-shit	111 to 50	—	+
1180340	Non-coding	—	Deletion GT → G	—	—	+	+

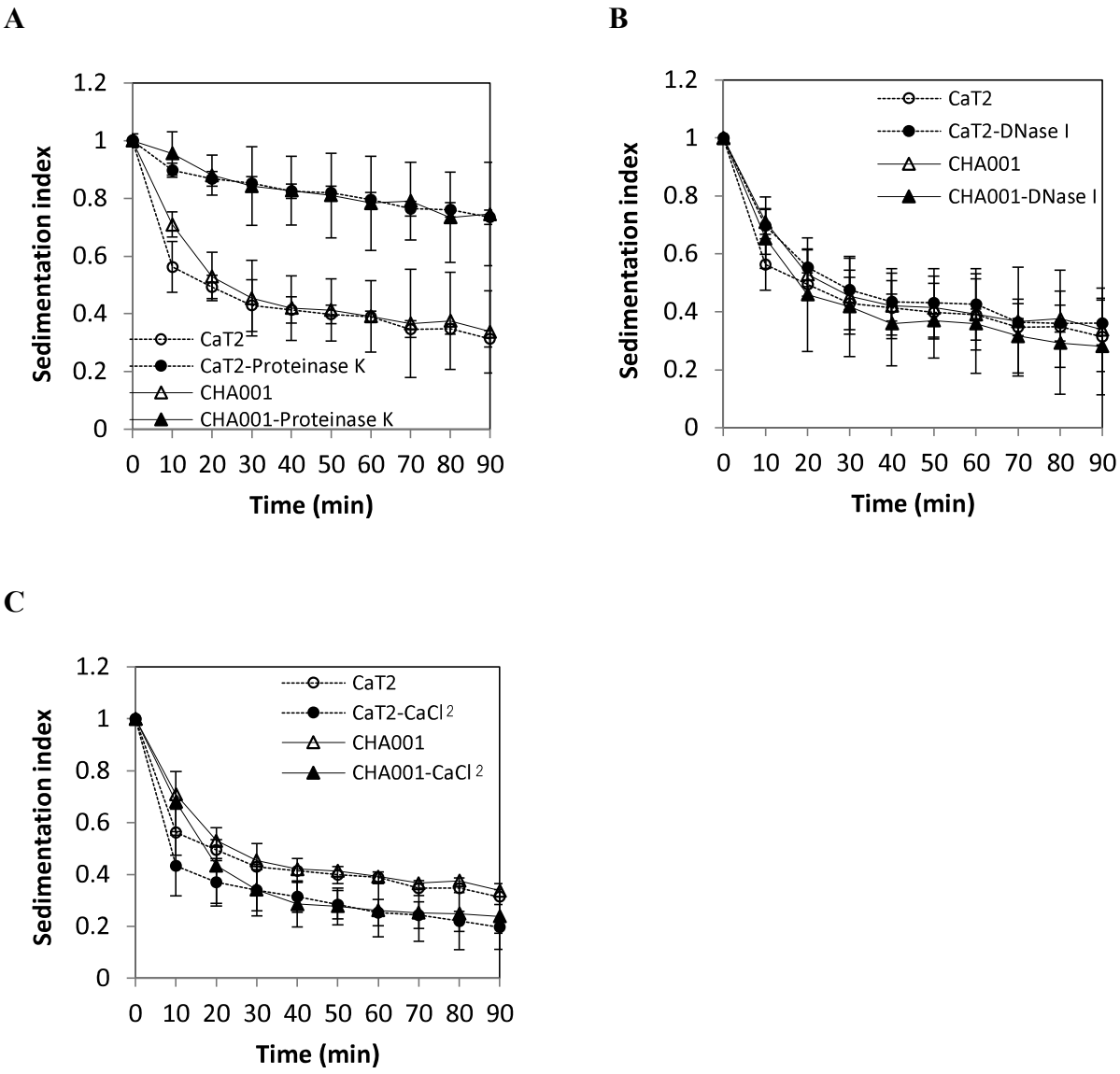

Fig. 2.4 Effects of proteinase K treatment, DNase treatment and addition of CaCl2 on the sedimentation indices of CaT2 and CHA001

CaT2 (circles) and aggregation-enhanced mutant CHA001 (triangles) were treated with proteinase K (A), DNase I (B) or $CaCl_2$ (C) (closed) or were left untreated (open) and then subjected to sedimentation analysis. Error bars represent standard deviations of the means of three independent experiments.

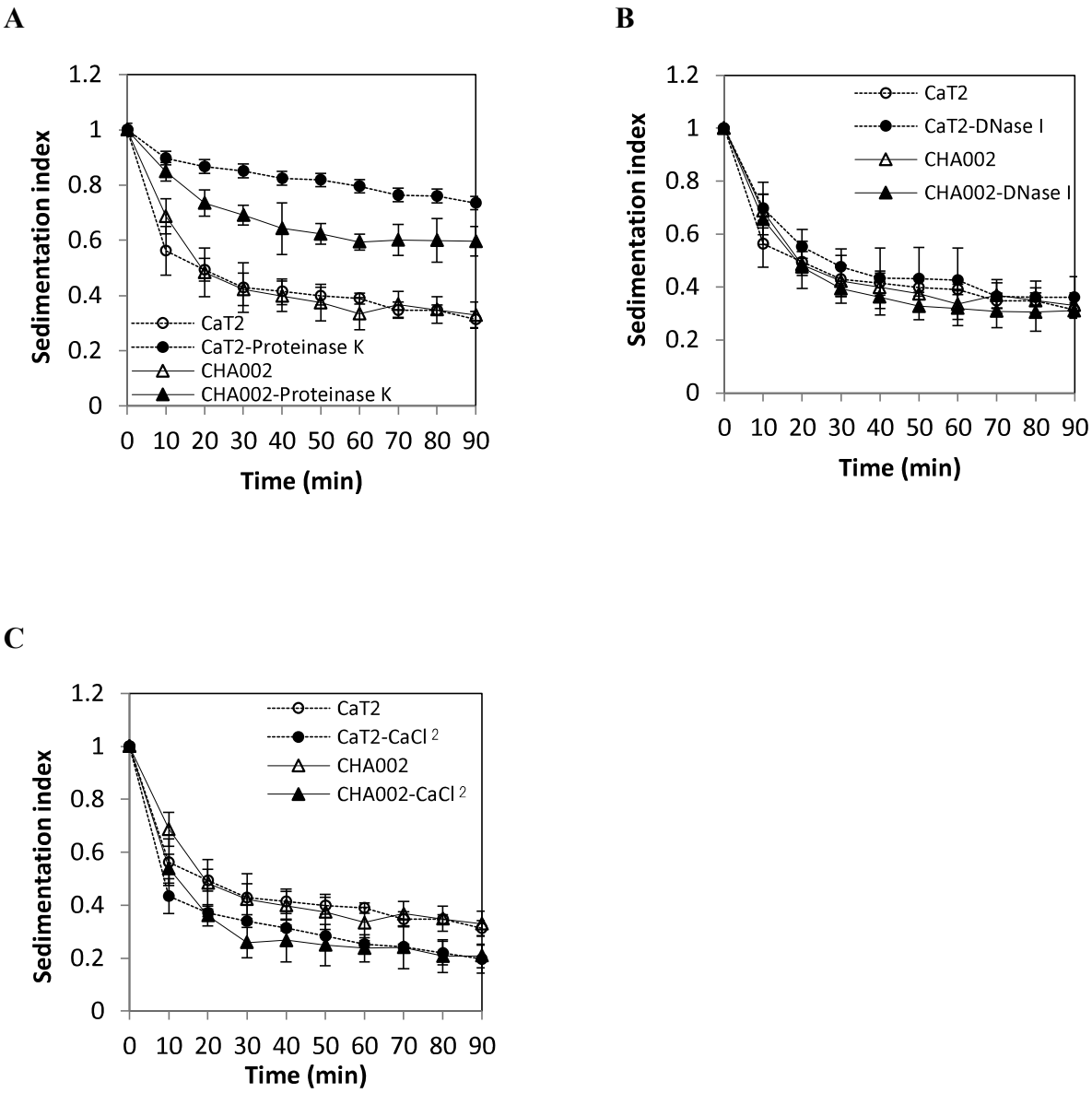

Fig. 2.5 Effects of proteinase K treatment, DNase treatment and addition of $CaCl_2$ on the sedimentation indices of CaT2 and CHA002

CaT2 (circles) and aggregation-enhanced mutant CHA002 (triangles) were treated with proteinase K (A), DNase I (B), or $CaCl_2$ (C) (closed) or were left untreated (open) and then subjected to sedimentation analysis. Error bars represent standard deviations of the means of three independent experiments.

2.4 DISCUSSION

Methanothermobacter sp. CaT2 possesses an extracellular protein, *MTCT_1020,* which is responsible for its aggregation (Sumikawa *et al.*, 2019) in addition to a surface sugar layer, which has been proposed to be involved in cell-cell interaction (Kosaka *et al*., 2014). The former has genetically been suggested, but additional aggregating factors have not been investigated. In this study, aggregation-enhanced mutants were isolated and characterized. TEM observations suggested that the isolated mutants, CHA001 and CHA002, have a surface sugar layer similar to that of CaT2 or slightly thinner, respectively, and have a cell wall slightly thinner or thinner than that of CaT2, respectively (Fig. 2.1 and Table 2.1). Such difference in these thicknesses may be due to mutations in the mutants. Treatment with proteinase K significantly reduced the sedimentation of both mutants. These findings suggest that the cell-cell interactions in aggregates of both mutants as well as in aggregates of CaT2 are mediated by extracellular proteins as core factors. However, CHA002, but not CHA001, aggregated to some extent even after proteinase K treatment (Fig. 2.5 A), suggesting the presence of another factor(s) for the aggregation of CHA002.

Genomic analysis revealed that CHA001 and CHA002 have three and four mutations, respectively (Table 2.2). In a previous study, seven genes were predicted to be responsible for the aggregation of CaT2 (Kosaka *et al*., 2014), but no mutations in these genes were found in either mutant (Table 2.2). Furthermore, although both mutants exhibited stronger aggregation than that of CaT2, there was no mutation in *MTCT_1020*. CHA001 and CHA002 share an amino acid substitution in MTCT_1348 (UniProt: T2GJ51), which is annotated to be a pyridoxamine 5'-phosphate oxidase. However, the protein may play a different role than the annotated enzyme. The domain analysis suggested that its function is unclear and the domain IPR011576 of the protein appears to be unrelated to the catalysis of pyridoxamine 5′-phosphate oxidase. This

mutation appears to strengthen the interaction by extracellular proteins because proteinase K treatment caused CHA001 to disperse aggregates to a level similar to that of CaT2 treated with proteinase K (Fig. 4 A). Therefore, the missense mutation of *MTCT_1348* may strengthen the protein-based interaction of CaT2 cells directly by the amino-acid substituted MTCT_1348, indirectly by increasing the expression of *MTCT_1020* or by increasing the activity of MTCT_1020 via protein–protein interaction. The possibility of the contribution of the nonsense mutation of *MTCT_0393* to the enhanced aggregation in CHA001 should not be ignored. The *MTCT_0393* gene encoding an ATP-binding subunit of the ABC cobalt transporter may form an operon with *MTCT_0394* for cobaltochelatase and *MTCT_0390* for magnesium chelatase. The mutation in *MTCT_0393* may affect the cobalt uptake of CHA001 from the environment and might cause the enhanced aggregation phenotype of CHA001 because cobalt is important for methanogen growth, especially on *Methanothermobacter* species (Murray *et al*., 1981; Schönheit *et al*., 1979). CHA002 may have an additional factor(s) responsible for the remaining aggregation capability after proteinase K treatment. It is thus assumed that the factor(s) is not a protein. The remaining aggregation capability was provided by either a nonsense mutation in *MTCT_0179* or a frame-shift mutation in *MTCT_0445*. MTCT_0179 (UniProt: T2GIP8) is annotated as acetyl-CoA synthetase but the BLAST search suggested that MTCT_1462 and MTCT_0630 are also acetyl-CoA synthetases because the identical homologies of their amino acid sequences with MTCT_0179 were 55% and 32%, respectively. Therefore, the activity for acetyl-CoA synthesis is conceivably complemented by the two paralogous proteins in CHA002. On the other hand, MTCT_0445 (UniProt: T2GI40) is an unknown membrane protein with three times the membrane-spanning segments and the mutation in CHA002 probably disrupts the function of MTCT_0445. The disruption is assumed to cause the thinner membrane and surface sugar layer in CHA002, resulting in the enhancement of cell aggregation. However, there is no evidence to support these assumptions. At least we can conclude that there is a non-proteinous

material(s) as an aggregation factor, which seems to be emphasized by a mutation(s), in addition to the main extracellular proteins for aggregation in CaT2.

CONCLUSION

Throughout chapters 1 and 2, it is provided that thermophilic hydrogenotrophic methanogen *Methanothermobacter* sp. CaT2 utilizes a large extracellular protein encoded by MTCT_1020 as a main aggregation factor, presumably with other extracellular protein(s) (Supplemental Figure). The aggregation seems to be enhanced by divalent cation(s) such as Ca^{2+} probably by interaction with these proteins. Furthermore, as ancillary factor(s), CaT2 has non-proteinous material(s) such as surface sugar layer to make up aggregation. However, effects of environments such as cell density or accumulated stress on such aggregation factors is still unclear. For example, *Pseudomonas aeruginosa* produces QS signal molecules when the stage of biofilm development is matured (Solano *et al*., 2014) and *A. fulgidus* responds to environmental stresses and forms biofilm (LaPaglia and Hartzell, 1997). In CaT2, there is no information about QS though the aggregation becomes stronger under salt stress conditions (data not shown). CaT2 would also have a QS communication and stress response for the aggregation. Further studies on the structure of MTCT_1020 product, the function of divalent cation(s), or environmental effects are needed to understand the detailed aggregation mechanisms of CaT2.

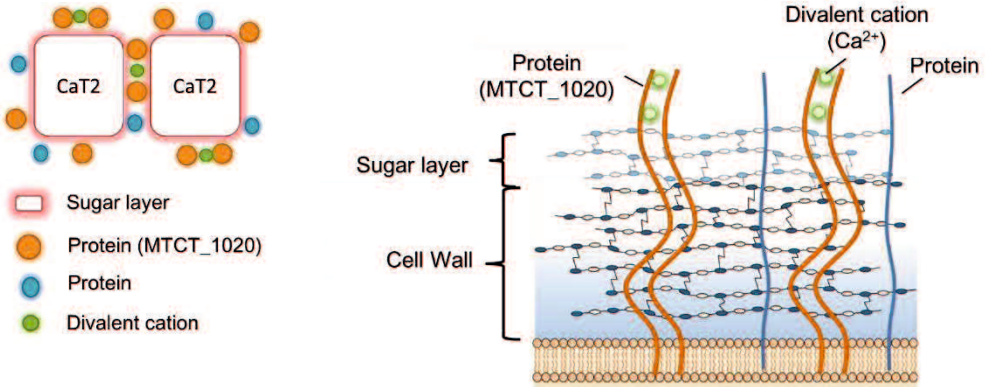

Supplemental Fig. A model of CaT2 aggregation mechanism.
Extracellular proteins as main factor(s) and polysaccharide on the cell surface as ancillary factor(s) are involved in the aggregation of CaT2. Divalent cations may interact with extracellular proteins to strengthen cell aggregation.

REFERENCES

Abdel-Nour, M., C. Duncan, A. Prashar, C. Rao, C. Ginevra, S. Jarraud, D.E. Low, A.W. Ensminger, M.R. Terebiznik, and C. Guyard. 2014. The Legionella pneumophila collagen-like protein mediates sedimentation, autoaggregation, and pathogen-phagocyte interactions. Appl. Environ. Microbiol. 80:1441–1454.

Ahring B.K.1995. Methanogenesis in thermophilic biogas reactors. Anton. Leeuw. 67:91–102

Akuzawa S., Nagaoka J., Kanekatsu M., Kanesaki Y., Suzuki T. 2016. Draft genome sequence of *Oceanobacillus picturae* Heshi-B3, isolated from fermented rice bran in a traditional japanese seafood dish. Genome Announc. 04;4

Alsteens D., P. Van Dijck, P.N. Lipke, and Y.F. Dufrêne. 2013. Quantifying the forces driving cell-cell adhesion in a fungal pathogen. Langmuir 29:13473–13480.

Bang C., C. Ehlers, A. Orell, D. Prasse, M. Spinner, S.N. Gorb, S.-V. Albers, and R.A. Schmitz. 2014. Biofilm formation of mucosa-associated methanoarchaeal strains. Front. Microbiol. 5:353.

Bodelón G., C. Palomino, and L.Á. Fernández. 2013. Immunoglobulin domains in Escherichia coli and other enterobacteria: from pathogenesis to applications in antibody technologies. FEMS Microbiol. Rev. 37:204–250.

Chong S., T.K. Sen, A. Kayaalp, and H.M. Ang. 2012. The performance enhancements of upflow anaerobic sludge blanket (UASB) reactors for domestic sludge treatment--a state-of-the-art review. Water Res. 46:3434–3470.

Claessen D., D. E. Rozen, O.P. Kuipers, L. Sogaard-Andersen, and G.P. van Wezel. 2014. Bacterial solutions to multicellularity: a tale of biofilms, filaments and fruiting bodies. Nature Rev. 12:115-124

El-Kirat-Chatel S., A. Beaussart, S.P. Vincent, M.A. Flos, P. Hols, P.N. Lipke, and Y.F. Dufrêne. 2015. Forces in yeast flocculation. Nanoscale 7:1760–1767.

Fernández N., E.E. Díaz, R. Amils, and J.L. Sanz. 2008. Analysis of microbial community during biofilm development in an anaerobic wastewater treatment reactor. Microb. Ecol. 56:121–132.

Finn R.D., J. Clements, and S.R. Eddy. 2011. HMMER web server: interactive sequence similarity searching. Nucleic Acids Res. 39:W29–37.

Finn R.D., J. Clements, W. Arndt, B.L. Miller, T.J. Wheeler, F. Schreiber, A. Bateman, and S.R. Eddy. 2015. HMMER web server: 2015 update. Nucleic Acids Res. 43:W30–8.

Flemming H.C., and J. Wingender. 2010. The biofilm matrix. Nat. Rev. Microbiol. 8:623–633.

Harada H., A. Ohashi, and H. Imachi. 2004. Realization of super high-rate methane fermentation bioreactor and rRNA-based molecular analysis of sludge consortium. J. Environ. Biotechnol. 4:19–27.

Hulshoff Pol, L.W., de Castro Lopes, S.I., Lettinga, G., and Lens,P.N. 2004. Anaerobic sludge granulation. Water Res. 38: 1376–1389.

Hirokawa Y., Kanesaki Y., Arai S., Saruta F., Hayashihara K., Murakami A., Shimizu K., Honda H., Yoshikawa H., Hanai T. 2018. Mutations responsible for alcohol tolerance in the mutant of *Synechococcus elongatus* PCC 7942 (SY1043) obtained by single-cell screening system. J. Biosci. Bioeng. 125:572–577.

Ishii S., T. Kosaka, K. Hori, Y. Hotta, and K Watanabe. 2005. Coaggregation facilitates interspecies hydrogen transfer between *Pelotomaculum thermopropionicum* and *Methanothermobacter thermautotrophicus*. Appl. Environ. Microbiol. 71: 7838-7845

Jarrell K.F., M. Stark, D.B. Nair, and J.P. Chong. 2011. Flagella and pili are both necessary for efficient attachment of *Methanococcus maripaludis* to surfaces. FEMS Microbiol. Lett. 319:44–50.

Kaspar H.F. and K. Wuhrmann.1978a. Product inhibition in sludge digestion. Microb. Ecol. 4:241–248.

Kaspar H.F. and K. Wuhrmann.1978b. Kinetic parameters and relative turnovers of some important catabolic reactions in digesting sludge. Appl. Environ. Microbiol. 36:1–7.

Kawakami Y., N. Hayashi, M. Ema, and M. Nakayama. 2007. Effects of divalent cations on *Halobacterium salinarum* cell aggregation. J. Biosci. Bioeng. 104:42–46.

Kobayashi O., N. Hayashi, R. Kuroki, and H. Sone. 1998. Region of FLO1 proteins responsible for sugar recognition. J. Bacteriol. 180:6503–6510.

Kosaka T., H. Toh, and A. Toyoda. 2013. Complete genome sequence of a thermophilic hydrogenotrophic methanogen, *Methanothermobacter* sp. strain CaT2. Genome Announc. 1:e00672–13.

Kosaka T., H. Toh, A. Fujiyama, Y. Sakaki, K. Watanabe, X.Y. Meng, S. Hanada, and A. Toyoda. 2014. Physiological and genetic basis for self-aggregation of a thermophilic hydrogenotrophic methanogen, *Methanothermobacter* strain CaT2. Environ. Microbiol. Rep. 6:268– 277.

LaPaglia C. and P.L. Hartzell. 1997. Stress-Induced Production of Biofilm in the Hyperthermophile *Archaeoglobus fulgidus*. Appl. Environ. Microbiol. 63:3158-3163.

LaPara T.M. and J.E. Alleman. 1999. Thermophilic aerobic biological wastewater treatment. Water Res. 33: 895-908.

Li H. and R. Durbin. 2009. Fast and accurate short read alignment with Burrows-Wheeler transform. Bioinformatics 25:1754–1760.

Liu W.T., O.C. Chan, and H.H. Fang. 2002. Characterization of microbial community in granular sludge treating brewery wastewater. Water Res. 36:1767–1775.

Liu Y., H.L. Xu, S.F. Yang, and J.H. Tay. 2003. Mechanisms and models for anaerobic granulation in upflow anaerobic sludge blanket reactor. Water Res. 37:661–673.

Liu Y.Q., Y. Liu, and J.H. Tay. 2004. The effects of extracellular polymeric substances on the formation and stability of biogranules. Appl. Microbiol. Biotechnol. 65:143–148.

Matsutani M., H. Suzuki, T. Yakushi, and K. Matsushita. 2014. Draft genome sequence of *Gluconobacter thailandicus* NBRC 3257. Stand. Genomic Sci. 9:614–623.

McKenna A., M. Hanna, E. Banks, A. Sivachenko, K. Cibulskis, A. Kernytsky, K. Garimella, D. Altshuler, S. Gabriel, M. Daly, and M.A. DePristo. 2010. The Genome Analysis Toolkit: a MapReduce framework for analyzing next-generation DNA sequencing data. Genome Res. 20:1297–1303.

Miki B.L., N.H. Poon, A.P. James, and V.L. Seligy. 1982. Possible mechanism for flocculation interactions governed by gene FLO1 in Saccharomyces cerevisiae. J. Bacteriol. 150:878–889.

Murray W.D. and Van Den Berg L. 1981. Effects of nickel, cobalt, and molybdenum on performance of methanogenic fixed-film reactors. Appl. Environ. Microbiol. 42:502–505.

Nakamura K., H. Tamaki, M.S. Kang, H. Mochimaru, S.-T. Lee, K. Nakamura, and Y. Kamagata. 2011. A six-well plate method: Less laborious and effective method for cultivation of obligate anaerobic microorganisms. Microbes Environ. 26:301‑306.

Okshevsky M., V.R. Regina, and R.L. Meyer. 2015. Extracellular DNA as a target for biofilm control. Curr. Opin. Biotech. 33:73-80

Orell A., S. Fröls, and S.V. Albers. 2013. Archaeal biofilms: the great unexplored. Annu. Rev. Microbiol. 67:337–354.

Pevere A., G. Guibaud, E.D. van Hullebusch, W. Boughzala, and P.N.L. Lens. 2007. Effect of Na^{+} and Ca^{2+} on the aggregation properties of sieved anaerobic granular sludge. Coll. Surf. A 306:142–149.

Robinson R.W., H.C. Aldrich, S.F. Hurst, and A.S. Bleiweis. 1985. Role of the cell surface of *Methanosarcina mazei* in cell aggregation. Appl. Environ. Microbiol. 49:321–327.

Salehizadeh H. and S.A. Shojaosadati. 2001. Extracellular biopolymeric flocculants: recent trends and biotechnological importance. Biotechnol. Adv. 19:371–385.

Samuel B.S., Hansen E.E., Manchester J.K., Coutinho P.M., Henrissat B., Fulton R., Latreille P., Kim K., Wilson R.K., and Gordon J.I. 2007. Genomic and metabolic adaptations of *Methanobrevibacter smithii* to the human gut. Proc. Natl. Acad. Sci. U.S.A. 104:10643–10648.

Satoh H., Y. Miura, I. Tsushima, and S. Okabe. 2007. Layered structure of bacterial and archaeal communities and their in situ activities in anaerobic granules. Appl. Environ. Microbiol. 73:7300–7307.

Schink B. 1997. Energetics of syntrophic cooperation in methanogenic degradation. Microbiol. Mol. Biol. Rev. 61:262–280

Schmidt J.E. and B.K. Ahring. 1993. Effects of magnesium on thermophilic acetate-degrading granules in upflow anaerobic sludge blanket (UASB) reactors. Enzyme Microb. Technol. 15:304–310.

Schmidt J.E. and B.K. Ahring. 1995. Granulation in thermophilic upflow anaerobic sludge blanket (UASB) reactors. Anton. Leeuw. 68:339–344.

Schmidt J.E. and B.K. Ahring. 1996. Granular sludge formation in upflow anaerobic sludge blanket (UASB) reactors. Biotechnol. Bioeng. 49:229–246.

Schneider C.A., Rasband W.S., Eliceiri K.W. 2012. NIH Image to ImageJ: 25 years of image analysis. Nat. Methods. 9:671–675.

Schönheit P., Moll J., and Thauer R.K. 1979. Nickel, cobalt, and molybdenum requirement for growth of *Methanobacterium thermoautotrophicum*. Arch. Microbiol. 123:105–107.

Seghezzo L., G. Zeeman, Jules B. van Lier, H.V.M. Hamelers, and G. Lettinga. 1998. A review: The anaerobic treatment of sewage in UASB and EGSB reactors. Bioresource Technol. 65:175-190

Sekiguchi Y., Y. Kamagata, K. Nakamura, A. Ohashi, and H. Harada. 1999. Fluorescence in situ hybridization using 16S rRNA-targeted oligonucleotides reveals localization of methanogens and selected uncultured bacteria in mesophilic and thermophilic sludge granules. Appl. Environ. Microbiol. 65:1280–1288.

Shahadat M., T.T. Teng, M. Rafatullah, Z.A. Shaikh, T.R. Sreekrishnan, and S.W. Ali. 2017. Bacterial bioflocculants: A review of recent advances and perspectives. Chem. Eng. J. 328:1139–1152.

Solano C., M. Echeverz, and I. Lasa. 2014. Biofilm dispersion and quorum sensing. Current Opinion in Microbiol. 18:96-104.

Spraggon G., Koesema E., Scarselli M., Malito E., Biagini M., Norais N., Emolo C., Barocchi M. A., Giusti F., Hilleringmann M., Rappuoli R., Lesley S., Covacci A., Masignani V., and Ferlenghi I. 2010. Supramolecular organization of the repetitive backbone unit of the Streptococcus pneumoniae pilus. PLoS One 5:e10919.

Sumikawa K., Kosaka T., Mayahara N., Matsutani M., Udo K., and Yamada M. 2019. An aggregation-defective mutant of *Methanothermobacter* sp. CaT2 reveals unique protein-dependent aggregation. Microbes Environ. 34:244-251.

Sumikawa K., Kosaka T., Udo K., Kanesaki Y., Yoshikawa H., and Yamada M. 2020. Characteristics of Physiology of and Genomic Mutations in Aggregation-enhanced Mutants of *Methanothermobacter* sp. CaT2. Biosci Biotechnol Biochem. doi: 10.1080/09168451.2019.1709790

Tiwari M.K., S. Guha, C.S. Harendranath, and S. Tripathi. 2006. Influence of extrinsic factors on granulation in UASB reactor. Appl. Microbiol. Biotechnol. 71:145-154.

Uemura S. and H. Harada. 1993. Microbial characteristics of methanogenic sludge consortia developed in thermophilic UASB reactors. Appl. Microbiol. Biotechnol. 39:654–660.

Ueno Y., S. Haruta, M. Ishii, and Y. Igarashi. 2001. Changes in product formation and bacterial community by dilution rate on carbohydrate fermentation by methanogenic microflora in continuous flow stirred tank reactor. Appl. Microbiol. Biotechnol. 57:65–73.

Van Lier J. B., J. L. S. Martin, and G. Lettinga. 1996. Effect of temperature on the anaerobic thermophilic conversion of volatile fatty acids by dispersed and granular sludge. Water Res. 30:199–207

Veiga M.C., M.K. Jain, W. Wu, R.I. Hollingsworth, and J.G. Zeikus. 1997. Composition and role of extracellular polymers in methanogenic granules. Appl. Environ. Microbiol. 63:403–407.

Verstrepen K.J., T.B. Reynolds, and G.R. Fink. 2004. Origins of variation in the fungal cell surface. Nat. Rev. Microbiol. 2:533–540.

Wang J. and C. Chen. 2006. Biosorption of heavy metals by Saccharomyces cerevisiae: A review. Biotechnol. Adv. 24:427–451.

Watrin L. and D. Prieur. 1996. UV and ethyl methanesulfonate effects in hyperthermophilic archaea and isolation of auxotrophic mutants of Pyrococcus strains. Curr. Microbiol. 33:377–382.

Wu W.-M., M.K. Jain, E.C. De Macario, J.H. Thiele, and J.G. Zeikus. 1992. Microbial composition and characterization of prevalent methanogens and acetogens isolated from syntrophic methanogenic granules. Appl. Microbiol. Biotechnol. 38:282–290.

Zinder S.H., S.C. Cardwell, T. Anguish, M. Lee, and M. Koch. 1984. Methanogenesis in a thermophilic (58°C) anaerobic digestor: Methanothrix sp. as an important aceticlastic methanogen. Appl. Environ. Microbiol. 47:796–807.

LIST OF PUBLICATIONS

1 **Kana Sumikawa**, Tomoyuki Kosaka, Noriaki Mayahara, Minenosuke Matsutani, Koichi Udo, and Mamoru Yamada: An Aggregation-defective Mutant of *Methanothermobacter* sp. CaT2 Reveals Unique Protein-dependent Aggregation

Microbes and Environments, Vol. 34 (2019), No. 3 pp. 244-251

(CHAPTER 1)

2 **Kana Sumikawa**, Tomoyuki Kosaka, Koichi Udo, Yu Kanesaki, Hirofumi Yoshikawa, and Mamoru Yamada: Characteristics of Physiology of and Genomic Mutations in Aggregation-enhanced Mutants of *Methanothermobacter* sp. CaT2

Bioscience, Biotechnology, and Biochemistry, (2020), doi: 10.1080/09168451.2019.1709790

(CHAPTER 2)